antioxidants

MDPI

Article

Tissue-Specific Adaptive Mechanisms of Amino Acid–Microbial Interactions in Earthworms Under Cadmium Stress: Neuro-Related Amino Acid Homeostasis and Metabolic Reprogramming of Sulfur-Containing and Branched-Chain Amino Acids

Yucui Ning, Hongyan Wang, Jiamin Su, Jiayi Gong, Guoqing Wang and Dongxing Zhou *

College of Resources and Environmental Science, Northeast Agricultural University, Harbin 150030, China; yucuining@neau.edu.cn (Y.N.); s240201055@neau.edu.cn (H.W.); s2502012030@neau.edu.cn (J.S.); a03240311@neau.edu.cn (J.G.); wgq7799@163.com (G.W.)
* Correspondence: zhouboshi@neau.edu.cn

Abstract

The mechanisms by which tissue functional differentiation coordinates amino acid metabolism in soil animals under cadmium (Cd) stress, and their potential associations with microorganisms, remain unclear. This study investigated the dynamic responses of amino acid metabolism in anterior and posterior tissues of *Eisenia fetida* exposed to Cd concentrations of 0–500 mg/kg for 1–30 days. Anterior tissues primarily exhibited imbalances in excitatory (Asp, Glu) and aromatic (Phe, Tyr) amino acids, suggesting disrupted neuro-related metabolic homeostasis. Changes in sulfur-containing amino acids (Met, Cys), branched-chain amino acids (Ile, Leu, Val), and histidine (His) in posterior tissues suggested their potential involvement in thiol buffering, energy metabolism adjustment, and metal chelation. TOPSIS analysis revealed three stages—stress compensation, enhanced defense, and functional disturbance—and identified stage-specific candidate amino acid biomarkers. Spearman correlation and path analyses showed that genera including Escherichia were associated with neuro-related amino acids in anterior tissues, whereas genera including Paracoccus were associated with sulfur-containing amino acids, branched-chain amino acids, and His in posterior tissues. These findings support a tissue-coordinated response framework of "central protection–peripheral detoxification," providing a basis for understanding heavy metal adaptation in soil animals and developing stage-specific biological early-warning strategies.

Keywords: cadmium; *Eisenia fetida*; amino acid metabolic reprogramming; TOPSIS analysis; path analysis; amino acid–microbial associations

Academic Editor: Claus Jacob

Received: 28 October 2026
Revised: 16 November 2026
Accepted: 18 November 2026
Published: 19 November 2026

Copyright: © 2026 by the authors. Licensee MDPI, Basel, Switzerland. This article is an open access article distributed under the terms and conditions of the Creative Commons Attribution (CC BY) license.

1. Introduction

Heavy metal cadmium (Cd) has become a priority control pollutant in the remediation of contaminated farmland and industrial site soils in China due to its high toxicity, strong bioaccumulation potential, and food chain amplification effects [1–3]. Earthworms, as "ecological engineers" of the soil ecosystem, are highly sensitive to Cd stress and represent the most widely used model organism in ecotoxicological research [4,5]. Existing

studies have shown that Cd stress can induce reactive oxygen species (ROS) bursts in earthworms, disrupt cellular redox homeostasis, interfere with energy metabolism pathways, and activate defense mechanisms such as metallothionein synthesis and antioxidant enzyme systems [6,7]. However, the vast majority of current studies focus on the whole-organism level or metabolic responses at a single time point, neglecting the metabolic heterogeneity arising from the functional differentiation of earthworm tissues, and failing to elucidate the metabolic coordination mechanisms among tissues at different stages. This has led to an insufficient understanding of the molecular nature underlying the long-term toxic effects of Cd, making it difficult to support the accurate risk assessment of soil heavy metal pollution.

Eisenia fetida exhibits distinct physiological functional zoning within its body: the anterior tissues are enriched with cerebral ganglia and peripheral nerve fibers, serving as the center for sensing environmental stress and regulating physiological activities; the posterior tissues are predominantly composed of muscle tissue, digestive tract, and excretory organs, performing core functions of locomotion, energy metabolism, substance excretion, and detoxification of exogenous pollutants [8]. This functional differentiation dictates that the anterior and posterior tissues must adopt differentiated metabolic strategies in response to Cd stress. Previous studies have found that the antioxidant enzyme activities in the anterior and posterior tissues of earthworms show significant differences in their responses to Cd stress [5,9]. However, to date, no study has systematically revealed the metabolic network regulatory mechanisms underlying such differences, particularly the tissue-specific evolution patterns of amino acid metabolism in connecting core processes such as protein synthesis, energy metabolism, and detoxification defense.

Amino acids are not only the basic building blocks of proteins but also key molecules involved in nerve signal transmission, redox balance regulation, heavy metal chelation, and energy supply within organisms [10–13]. For example, the disruption of glutamate (Glu) and aspartate (Asp) homeostasis directly mediates the neurotoxicity of heavy metals [14]; sulfur-containing amino acids (methionine, Met; cysteine, Cys) constitute the first line of defense in cellular antioxidant protection [15]; and the imidazole group of histidine (His) can form stable coordination complexes with heavy metal ions, making it an important natural heavy metal chelator in organisms [16,17]. However, current studies on amino acid metabolism in earthworms under Cd stress are mostly limited to the whole-body level or single-stress conditions, lacking a systematic understanding of the differentiation and dynamic evolution of amino acid metabolism in different functional tissues under Cd stress. Meanwhile, host metabolic changes do not occur in isolation, and the associated microorganisms may be closely linked to amino acid metabolic status. Moreover, it remains unclear whether the anterior and posterior tissues of earthworms exhibit different amino acid response trajectories under Cd stress, and what associations exist between these tissue-specific metabolic changes and microbial taxa. More importantly, the identification of toxicological response stages currently relies largely on existing knowledge or standard protocols (e.g., ISO, OECD), which essentially amounts to subjective scientific hypotheses proposed by researchers [18–20]. This widely overlooked knowledge gap undermines the rigor and ecological relevance of related conclusions. Therefore, there is an urgent need to employ methodological innovation and conceptual reconstruction to resolve amino acid metabolic responses at the tissue level and examine their potential associations with microbial taxa, so as to further elucidate the life-maintenance mechanisms of earthworms under stress, promote the shift from understanding individual oxidative stress effects to ecological homeostasis mechanisms, and contribute to a more comprehensive understanding of the metabolic adaptation strategies of earthworms under Cd stress.

Accordingly, this study selected *Eisenia fetida* as the research subject and, by setting different Cd stress concentrations (0–500 mg/kg) at different time points (1–30 d), systematically analyzed the dynamic responses of 17 amino acids in the anterior and posterior tissues, revealing the spatiotemporal responses and functional differentiation of amino acid metabolism in the anterior and posterior segments during Cd stress. Through TOPSIS comprehensive evaluation, the key responsive amino acids at different stages of Cd stress were identified, and the metabolic trajectory, evolving from early compensation to late functional disorder, was elucidated. In addition, Spearman correlation and path analyses of amino acids and microbial taxa under selected key stress conditions were conducted to characterize tissue-specific association patterns and key statistical pathways between amino acids and microbial taxa. The novelty of this study lies in integrating tissue-specific amino acid dynamics with microbial community characteristics under selected key stress conditions, thereby revealing potential associations between host metabolic responses to Cd stress and tissue-associated microbial changes. The innovation of this study lies in the combination of molecular biostatistics and advanced mathematical modeling (MB-AMm), integrating the dynamic changes in amino acids in different tissues with the characteristics of microbial communities under key stress conditions, thereby revealing the potential associations between host metabolic responses and tissue-associated microbial changes under Cd stress. On this basis, from the three dimensions of tissue functional differentiation, metabolic resource reallocation, and microbial–metabolic associations, a tissue-coordinated response framework of "central protection–peripheral detoxification" was further constructed, providing tissue-resolution metabolic evidence for the mechanistic ecotoxicological analysis of Cd pollution and for stage-specific biological early warning.

2. Materials and Methods

2.1. Test Materials

2.1.1. Test Reagents

Cadmium was added in the form of $CdCl_2 \cdot 2.5H_2O$ (analytical grade), purchased from Tianjin Guangfu Technology Development Co., Ltd. (Tianjin, China). Peat was obtained from Harbin Flower Market (Harbin, China). Kaolin ($Ai_2O_3 \cdot 2SiO_2 \cdot 2H_2O$, analytical grade) was purchased from Tianjin Kermel Chemical Reagent Co., Ltd. (Tianjin, China). Quartz sand, with SiO_2 as its main component, was collected from a construction site as ordinary river sand.

Hydrochloric acid (6 mol/L) was purchased from Nanjing Jiancheng Bioengineering Institute (Nanjing, China). Liquid nitrogen (cryogenic refrigerant) was obtained from Nanjing Jiancheng Bioengineering Institute. Citrate buffer (pH 2.2) was purchased from Nanjing Jiancheng Bioengineering Institute. Ninhydrin (containing reducing agent) was originally imported from Sykam (Fürstenfeldbruck, Germany). The standard mixture of 18 hydrolyzed amino acids was originally imported from Sykam, Germany.

2.1.2. Artificial Soil

According to the standard methods provided by the OECD [21,22], the artificial soil was prepared as follows: peat, kaolin clay, and quartz sand were thoroughly mixed at a mass ratio of 1:2:7, the pH was adjusted to 6.0–6.5 with analytically pure calcium carbonate, and deionized water was added to adjust the soil moisture content to 40% of the maximum water-holding capacity.

2.1.3. Test Earthworms

The test earthworms, *Eisenia fetida*, were obtained from the Ecological Agriculture Science and Technology Backyard in Bin County, Heilongjiang Province, where they were

reared with decomposed cow dung as feed. Healthy adult earthworms, aged over two months, with a body weight of 300–500 mg and a distinct clitellum, were selected for the experiment. Prior to the experiment, the earthworms were acclimated for one week in an artificial climate chamber under conditions of 25 °C, 80% relative humidity, and continuous darkness, and were fed with decomposed cow dung every two days. After acclimation, the earthworms were transferred onto moist filter paper and subjected to gut clearance in the dark for 24 h to eliminate intestinal contents.

2.2. Experimental Design

Two groups of experiments were established: a long-term exposure group and a short-term exposure group. Based on the results of preliminary experiments and previous studies [23–25], six Cd concentration gradients were set: 0, 50, 100, 125, 250, and 500 mg/kg (on a dry soil basis).

The experiments were conducted in plastic boxes measuring 19 cm × 12.5 cm × 4.5 cm. Each box contained 200 g (wet weight) of artificial soil, and 10 gut-cleared earthworms were placed in each box. Cd^{2+} solutions of different concentration gradients were evenly sprayed onto the soil, thoroughly mixed, and then left to stand at room temperature for 48 h to allow the heavy metal to reach adsorption equilibrium in the soil. Subsequently, the soil moisture content was readjusted to 40% of the maximum water-holding capacity. Ten gut-cleared earthworms were placed into each container, and four biological replicates were set up for each treatment group. During the experimental period, the conditions were maintained at 25 °C, 80% relative humidity, and continuous darkness, with deionized water replenished every two days to maintain the soil moisture content.

2.3. Sample Collection and Processing

For the short-term exposure group, one earthworm was randomly collected from each container daily; for the long-term exposure group, one earthworm was randomly collected from each container every 10 days. After collection, the earthworms were depurated for 12 h under moist and dark conditions, rinsed with deionized water to remove surface debris, blotted dry with filter paper, and immediately stored in an ultra-low-temperature freezer at −80 °C until further analysis.

For sample processing, each earthworm was dissected into anterior (including the clitellum and the region anterior to it) and posterior (the region posterior to the clitellum) segments using a sterile scalpel under aseptic conditions, with the clitellum serving as the anatomical boundary. The two tissue segments were separately dried in a constant-temperature drying oven at 60 °C for 24 h to a constant weight and then accurately weighed (precision: 0.0001 g). Throughout the procedure, a strict one-earthworm–one-instrument–one-dissection protocol was followed to prevent cross-contamination.

2.4. Determination of Amino Acid Content

The concentrations of 17 hydrolyzed amino acids were determined by acid hydrolysis followed by amino acid analysis. The results represent the amino acids released from the tissue samples by acid hydrolysis and reflect their hydrolyzed amino acid composition. Accurately weighed dried tissue samples were placed in anaerobic hydrolysis tubes, and 5 mL of 6 mol/L hydrochloric acid was added. After thorough mixing, the tubes were frozen in liquid nitrogen, evacuated, and sealed. Hydrolysis was performed at a constant temperature of 110 °C for 24 h. After cooling, the hydrolysate was brought to a final volume of 10 mL with deionized water and filtered through a 0.45 μm aqueous membrane filter. A 1 mL aliquot of the filtrate was transferred to an EP tube and concentrated to dryness under vacuum, and the residue was redissolved in 1 mL of deionized water and dried again; this process was repeated twice to remove residual hydrochloric acid. Finally,

the residue was dissolved in 2 mL of sample dilution buffer (pH 2.2), filtered through a 0.22 μm aqueous membrane filter, and analyzed using an automatic amino acid analyzer (Sykam, Germany).

The analytical conditions were as follows: injection volume: 0.05 mL; chromatographic column: LCAK06/Na; detection wavelengths, 570 nm + 440 nm; mobile phases, sodium citrate A (0.12 mol/L, pH 3.45) and B (0.2 mol/L, pH 10.85); flow rates: 0.45 mL/min for the elution pump and 0.25 mL/min for the derivatization pump; temperature gradient from 58 °C to 74 °C; and pressure range of 30–40 bar. Quantification was performed using the external standard method, with qualitative identification based on the retention times of amino acid standards and quantitative determination based on peak areas.

2.5. TOPSIS Method

The TOPSIS (Technique for Order Preference by Similarity to Ideal Solution) method was used to comprehensively evaluate changes in amino acid contents in the anterior and posterior tissues of earthworms under different Cd stress conditions and to identify key responsive amino acids. Stress duration and stress concentration were used as the evaluation dimensions, and amino acid composition was used as the set of evaluation criteria. A feature matrix was constructed from the absolute percentage changes in the content of each amino acid relative to the control. Indicator weights were determined using the entropy weight method, and the resulting weight vector was then applied to the feature matrix. The specific steps were as follows:

For t cadmium exposure durations $P_1,P_2,...,P_t$ or c exposure concentrations $Q_1,Q_2,...Q_c$, as well as for n amino acid component indicators $X_1,X_2,X_3,...,X_n$, a characteristic matrix was constructed using the absolute values of the percentage changes in the contents of various amino acid components following cadmium stress.

$$P=\begin{bmatrix} y_{11} & \cdots & y_{1\mu} & \cdots & y_{1n} \\ \vdots & & \vdots & & \vdots \\ y_{\alpha 1} & \cdots & y_{\alpha\mu} & \cdots & y_{\alpha n} \\ \vdots & & \vdots & & \vdots \\ y_{t1} & \cdots & y_{t\mu} & \cdots & y_{tn} \end{bmatrix} \quad Q=\begin{bmatrix} z_{11} & \cdots & z_{1\mu} & \cdots & z_{1n} \\ \vdots & & \vdots & & \vdots \\ z_{\beta 1} & \cdots & z_{\beta\mu} & \cdots & z_{\beta n} \\ \vdots & & \vdots & & \vdots \\ z_{c1} & \cdots & z_{c\mu} & \cdots & z_{cn} \end{bmatrix}$$

$$\alpha=1,2,\cdots,t;\beta=1,2,\cdots,c;\mu=1,2,\cdots,n$$

Determine the positive ideal solution A_μ^+ and the negative ideal solution A_μ^-:

$$A_\mu^+=\max\left(\varepsilon_{1\mu},\varepsilon_{2\mu},\cdots,\varepsilon_{\eta\mu}\right) \qquad A_\mu^-=\min\left(\varepsilon_{1\mu},\varepsilon_{2\mu},\cdots,\varepsilon_{\eta\mu}\right)$$

where $\varepsilon_{\eta\mu}$ denotes $\varepsilon_{t\mu}$ and $\varepsilon_{c\mu}$, respectively:

$$\varepsilon_{t\mu}=\omega'_\mu\times y_{t\mu} \qquad \varepsilon_{c\mu}=\omega''_\mu\times z_{c\mu}$$

The entropy weight method was used to calculate the weights of each amino acid indicator separately for different stress durations and Cd concentrations. ω'_μ and ω''_μ are the weights of various amino acid component indicators under non-stress duration and under stress concentration, respectively.

The Euclidean distance is:

$$S_\eta^+=\sqrt{\sum_{\mu=1}^{n}\left(A_\mu^+-\varepsilon_{\eta\mu}\right)^2} \qquad S_\eta^-=\sqrt{\sum_{\mu=1}^{n}\left(A_\mu^--\varepsilon_{\eta\mu}\right)^2}$$

Change indices of various amino acids following cadmium stress: $ci_\eta = \frac{S_\eta^-}{S_\eta^+ + S_\eta^-}$.

The higher the ci_η value, the closer the overall amino acid composition under that treatment is to the positive ideal solution, indicating a greater overall change relative to the control. To facilitate comparison of each treatment's relative contribution to the overall change index, the TOPSIS results are expressed as percentages of the change index:

$$CI = \frac{ci_\eta}{\sum ci_\eta} \times 100\%, \qquad CI \in [0,1]$$

In this study, equal weights were assigned to Cd exposure duration and concentration, and both were treated as "lower-is-better" criteria. For each evaluation dimension, the *CI* values of the corresponding treatments were summed to obtain a composite change score for each exposure duration or concentration. These scores were used to compare the relative responses of amino acid composition under different stress conditions and to identify amino acids showing pronounced changes, as well as the key stress conditions. According to the magnitude of the change index (*CI*), the degree of change in amino acids under different stress conditions was classified into five levels: $0 < CI \leq 1$ indicated a highly significant change; $1 < CI \leq 4$ indicated a significant change; $4 < CI \leq 7$ indicated a moderate change; $7 < CI \leq 10$ indicated a slight change; and $CI > 10$ indicated that the amino acid content remained essentially unchanged compared with normal physiological metabolism [5]. The entire analysis was performed using the statistical software DPS 7.05.

2.6. Metagenomic Sequencing Analysis

Based on the TOPSIS analysis, the key stages following Cd exposure were identified, and earthworm and soil samples were collected at the corresponding stages. Samples from the same stage were pooled, and total genomic DNA was extracted from each sample for subsequent analysis. The OD260/280 ratio was measured using a NanoDrop spectrophotometer (Thermo Fisher Scientific Inc., Waltham, MA, USA) to assess DNA purity and ensure DNA integrity. Metagenomic sequencing was performed by Wuhan Bioyue Zhihe Biotechnology Co., Ltd. on the Illumina HiSeq™ 2000 platform. After sequencing, raw reads were first evaluated for base quality using FastQC, followed by quality filtering with Fastp v0.20. The filtered high-quality sequences were assembled using MEGAHIT, and the resulting contigs were dereplicated using CD-HIT with thresholds of 95% sequence identity and 90% coverage. Subsequently, MetaGeneMark was used to predict open reading frames (ORFs) from the dereplicated sequences, and ORFs shorter than 100 nt were removed to construct an initial non-redundant gene catalog. SOAPaligner was further employed for sequence alignment, and genes supported by at least 2 reads were retained as the non-redundant gene set (Unigenes). The amino acid sequences corresponding to the Unigenes were aligned against the NR and KEGG databases (BLASTP, E-value $< 1 \times 10^{-5}$) for taxonomic annotation and KEGG functional annotation, respectively.

Data processing, Spearman correlation analysis, and visualization were performed using R software (version 4.6.1), primarily with the readxl, dplyr, tidyr, Hmisc, ggplot2, and pheatmap packages. Under the key stress conditions identified by the TOPSIS comprehensive evaluation, Spearman's correlation coefficients (r) and significance levels (p) were calculated separately between the relative abundances of microbial genera and the contents of 17 amino acids in the anterior and posterior tissues. Correlation heatmaps were then generated to characterize tissue-specific amino acid-microbe association patterns. Path analysis was further performed using DPS 7.05, with the contents of key amino acids as dependent variables and the abundances of associated microorganisms as inde-

pendent variables. Direct path coefficients, indirect effects, and coefficients of determination (R^2) were calculated to elucidate the major microbe-amino acid association pathways and their tissue-specific differences [5].

3. Results and Discussion

3.1. Spatiotemporal Response Characteristics of Amino Acids in Earthworms Under Cadmium Stress

3.1.1. Baseline Dynamics of Total Amino Acid Content in the Control Group

In the control group, the total amino acid content in both the anterior and posterior tissues of earthworms exhibited natural fluctuations over time, but the fluctuation trends showed significant tissue-specific differences (Figure 1). The mean total amino acid content in the anterior tissue was significantly higher than that in the posterior tissue, exceeding it by an average of 18.6%, and the time required for the anterior tissue to return to the initial level was longer than that for the posterior tissue. These findings indicate that the metabolic homeostasis of the neural regulatory center is more sensitive to minor environmental changes, whereas the metabolic homeostasis of peripheral tissues possesses a stronger self-regulatory capacity.

In terms of composition, Glu and Asp in the posterior tissue exhibited highly synchronized fluctuation trends, and Glu consistently remained the most abundant amino acid. This pattern aligns with the high energy metabolism demands of the posterior tissue, as Glu and Asp may contribute to rapid ATP production through the tricarboxylic acid (TCA) cycle, supplying energy for muscle activity and material transport [26,27]. The sulfur-containing amino acids (Cys, Met) showed low initial levels but considerable fluctuation amplitudes, displaying an overall trend of an initial decrease followed by an increase. The branched-chain amino acid (Ile) and His exhibited a continuous upward trend, increasing by 29.2% and 39.6%, respectively, by the end of the experiment compared to the initial levels. Moreover, the magnitude of increase in the posterior tissue was significantly greater than that in the anterior tissue, suggesting that these amino acids may participate in processes such as growth, development, and antioxidant defense during the normal physiological metabolism of earthworms.

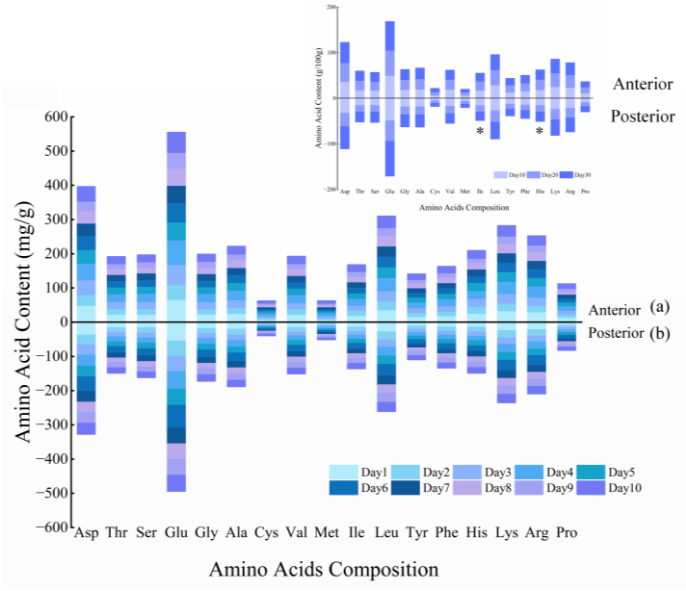


Figure 1. Changes in amino acid composition in earthworms under the control treatment. (Note: Amino Acid Contents in the Anterior and Posterior Segments of *Eisenia fetida* Under Control Conditions. Different Lowercase Letters Indicate Significant Differences in Total Amino Acid Content

Between the Two Tissues ($p < 0.05$). * Indicate Significant Differences in the Contents of Individual Amino Acids Between the Anterior and Posterior Segments ($p < 0.05$). Asp: Aspartic; Thr: Threonine; Ser: Serine; Glu: Glutamic; Gly: Glycine; Ala: Alanine; Cys: Cystine; Val: Valine; Met: Methionine; Ile: Ileucine; Leu: Leucine; Tyr: Tyrosine; Phe: Phenylalanine; His: Histidine; Lys: Lysine; Arg: Agrine; Pro: Proline).

3.1.2. Concentration-Dependent Response of Total Amino Acid Content Under Short-Term Exposure

Under short-term Cd exposure (1–10 d), the changes in total amino acid content in the anterior and posterior tissues of earthworms exhibited marked concentration-dependent characteristics (Figure 2). On the first day of exposure, the total amino acid content in all Cd-treated groups was significantly lower than that in the control group, and the magnitude of the decrease increased with rising Cd concentration. In the 50 mg/kg treatment group, the Glu content in the anterior tissue decreased by 22.1%, while six amino acids, including Ser and Cys, showed no significant changes in the posterior tissue. In the high-concentration treatment group (500 mg/kg), Asp and Glu in the posterior tissue decreased by 28.4% and 30.2%, respectively, whereas His was significantly elevated. These results suggest that the amino acid composition of earthworms may undergo rapid adjustment during the early stages of Cd exposure. Previous studies have shown that amino acids can contribute to the synthesis of defensive substances, such as metallothioneins and antioxidant enzymes, while their catabolism can also provide substrates for energy metabolism [28,29]. Therefore, amino acid changes in the anterior and posterior tissues may be associated with the earthworm's response to acute stress.

On day 5 of exposure, the response pattern of total amino acid content reversed: the total amino acid content in the 100 mg/kg and 250 mg/kg treatment groups was significantly higher than that in the control group, with Glu and Asp in the posterior tissue increasing by 58.5% and 59.0%, respectively, whereas no significant change was observed in the 500 mg/kg treatment group. This phenomenon reflects the activation of a stress compensation mechanism in earthworms: at low to moderate concentrations, the organism accelerates protein degradation and amino acid synthesis to replenish consumed metabolic substrates and maintain normal cellular physiological functions. In contrast, at high concentrations, Cd toxicity exceeds the compensatory capacity of the organism, inhibiting both protein synthesis and degradation, thereby keeping the total amino acid content at a relatively low level [30]. On day 10 of exposure, the total amino acid content peaked in the 500 mg/kg treatment group (485.69 mg/g in anterior tissues and 412.97 mg/g in posterior tissues), significantly exceeding that of all other treatment groups. Such pronounced alterations in amino acid composition under high-intensity Cd stress reflect a marked disturbance in protein and amino acid homeostasis, implying that the organisms had shifted from a state of compensatory adaptation to functional impairment [31,32].

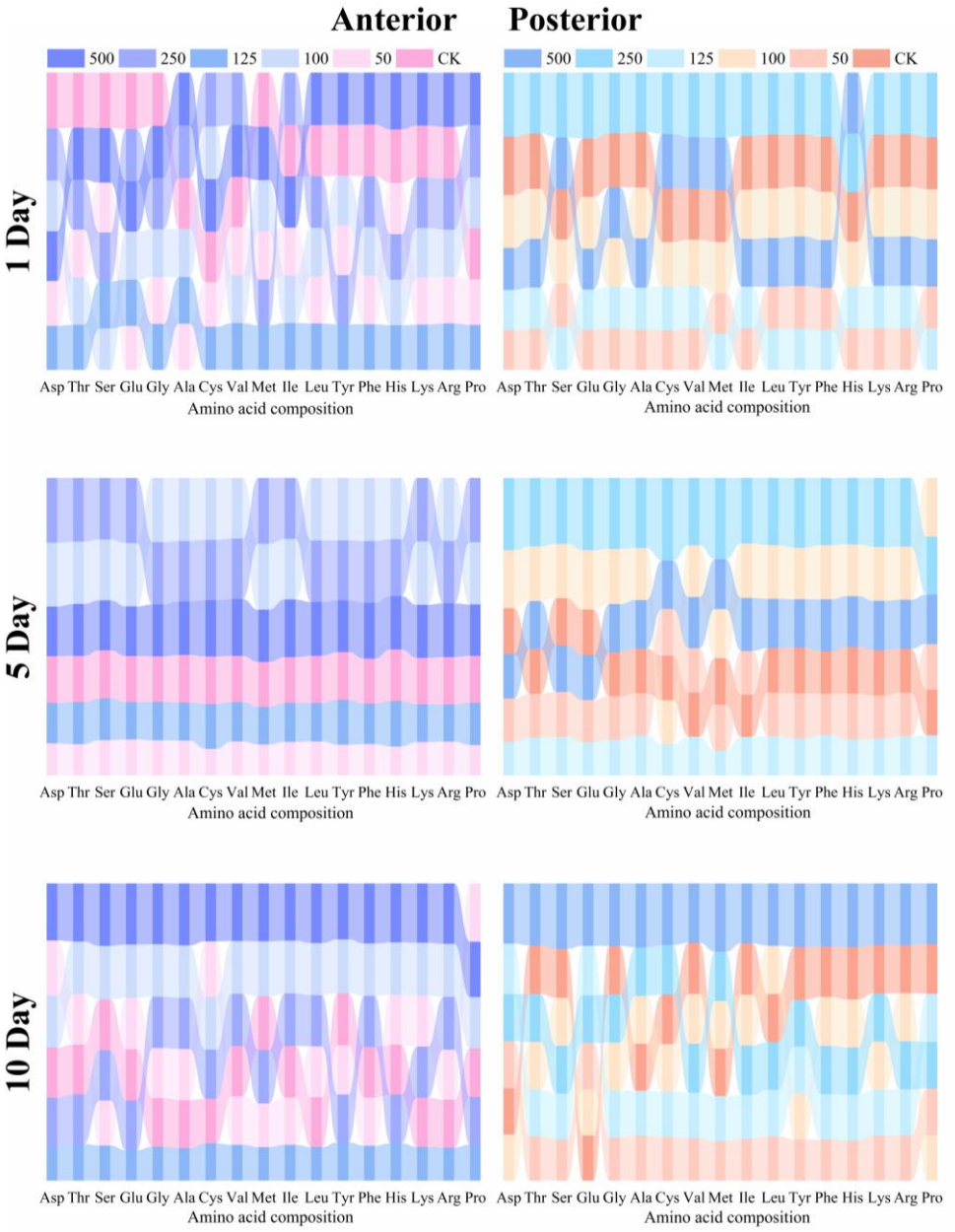


Figure 2. Effects of cadmium concentrations on total amino acid content in the anterior and posterior tissues of earthworms under short-term exposure.

3.1.3. Persistent Effects of Long-Term Exposure on Total Amino Acid Content

Under long-term Cd exposure (10–30 d), the changes in total amino acid content exhibited pronounced time-dependent cumulative effects and tissue specificity (Figure 3). In the 50 mg/kg low-concentration treatment group, after 10 d of exposure, the total amino acid content in the posterior tissue decreased significantly (with Cys and Tyr decreasing by 38.9% and 36.0%, respectively), while the anterior tissue remained largely unchanged. After 20 d of exposure, the total amino acid content in the anterior tissue decreased significantly, whereas in the posterior tissue, only four amino acids, including Cys and Val, showed decreases. After 30 d of exposure, the total amino acid content in both the anterior and posterior tissues decreased significantly, with Glu showing the greatest decrease of 44.6%. This dynamic process indicates that under low-concentration Cd stress, the posterior tissue, serving as the peripheral detoxification site, is the first to bear the metabolic detoxification burden of Cd. With prolonged exposure, Cd gradually accumulates in the

anterior tissue, leading to the disruption of metabolic homeostasis in the neural center [33,34].

In the 100 mg/kg and 250 mg/kg treatment groups, the total amino acid content in both the anterior and posterior tissues remained significantly lower than that in the control group throughout the entire exposure period, and the magnitude of the decrease in the anterior tissue was consistently greater than that in the posterior tissue. In the 500 mg/kg high-concentration treatment group, the total amino acid content in the anterior tissue at 10 d and in the posterior tissue at 20 d peaked, with His increasing by 31.9%. After 30 d of exposure, the contents of branched-chain amino acids such as Leu and Val in the posterior tissue recovered to control levels, whereas the contents of the other amino acids remained significantly reduced. These results suggest that under long-term high-concentration Cd stress, the metabolic defense system of earthworms is partially exhausted and can only maintain the functions of certain core metabolic pathways [35,36].

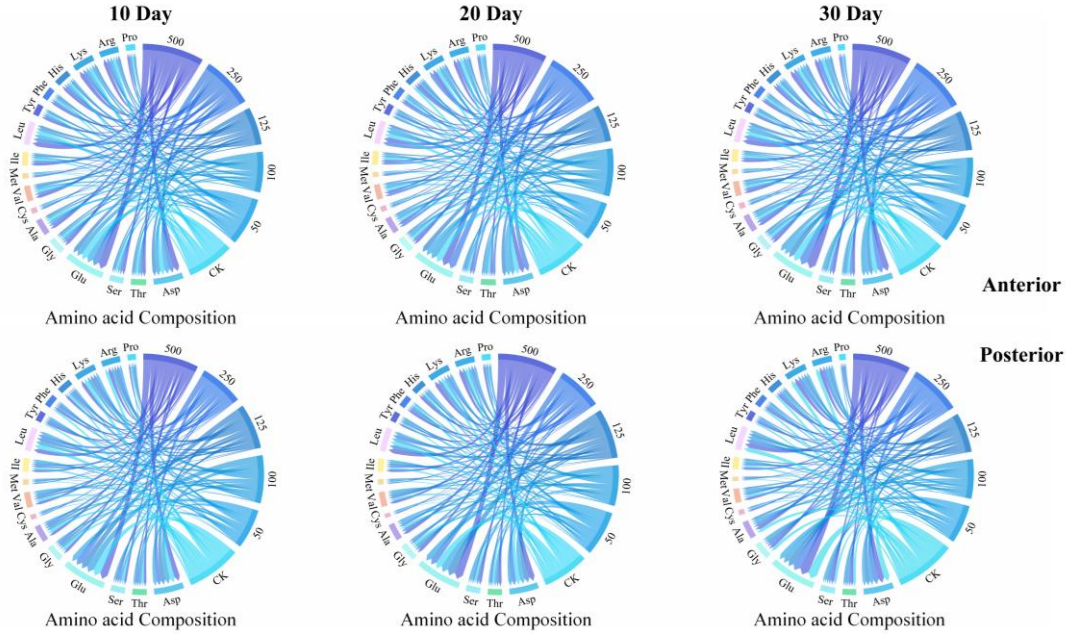


Figure 3. Changes in total amino acid content in the anterior and posterior tissues of earthworms under long-term cadmium stress.

3.2. Amino Acid Metabolic Reprogramming in the Anterior and Posterior Segments of Earthworms Under Cadmium Stress

3.2.1. Anterior Tissue: Homeostatic Remodeling of Neuro-Related Amino Acids

The TOPSIS analysis results (Figure 4) revealed that under low-concentration Cd stress (50–100 mg/kg), the most responsive amino acids in the anterior tissue were Asp, Glu, Phe, and Tyr, all of which are closely associated with neural function [37–39]. Combined with their temporal dynamics (Figure 4), Asp and Glu exhibited a significant decrease during the early exposure period (1–3 d), an abnormal rebound during the middle period (5–10 d), and remained persistently elevated under long-term exposure. Studies suggest that Cd ions may enter neurons through calcium channels and interfere with synaptic vesicle release, potentially reducing the levels of the excitatory neurotransmitters Asp and Glu in the synaptic cleft and impairing neurotransmission [40–44]. As stress duration increases, Cd-induced ROS bursts may exacerbate lipid peroxidation in neuronal membranes and increase membrane permeability, potentially causing large amounts of intracellular Asp and Glu to be released into the synaptic cleft and raising their concentrations above neurotoxic levels. Excess Glu may also overactivate NMDA (N-methyl-D-

aspartate) receptors, triggering excessive calcium influx and further ROS production [45–48], This may create a vicious cycle in which oxidative stress progresses to excitotoxicity, ultimately leading to neuronal apoptosis. This proposed mechanism may help explain the initial decrease followed by an increase in Asp and Glu observed in this study and provide relevant metabolite-based evidence for Cd neurotoxicity.

Furthermore, the metabolic disturbances of Phe and Tyr under long-term exposure also carry significant implications for neurotoxicity. Phe serves as a precursor to Tyr, which is in turn the substrate for the synthesis of monoamine neurotransmitters such as dopamine and norepinephrine [49]. In this study, Phe levels increased while Tyr levels decreased under long-term Cd exposure. This pattern may suggest that Cd inhibited phenylalanine hydroxylase activity, thereby limiting the conversion of Phe to Tyr. Changes in Phe and Tyr metabolism may affect the synthesis of monoamine neurotransmitters and, in turn, be associated with behavioral abnormalities such as reduced feeding and slower movement [50–54]. This interpretation is consistent with behavioral changes reported in earthworms exposed to Cd, although it requires further validation through measurements of relevant enzyme activities, neurotransmitter levels, and behavioral endpoints.

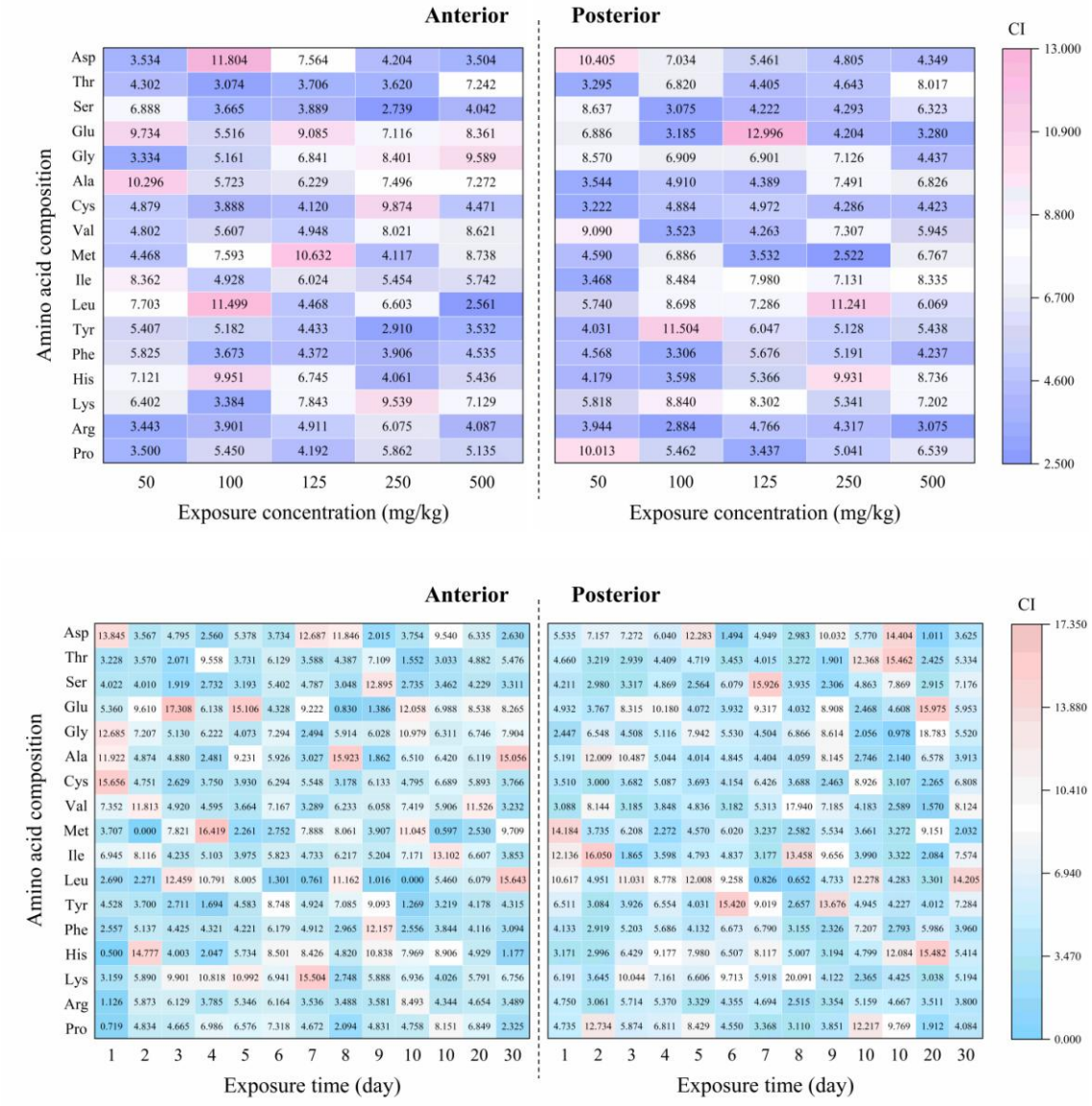


Figure 4. CI results of amino acid content in anterior and posterior segments of earthworm tissues under the dominance of concentration and time.

3.2.2. Posterior Tissue: Multi-Level Detoxification Metabolic Reprogramming

Unlike the anterior tissue, the most responsive amino acids in the posterior tissue were sulfur-containing amino acids (Met, Cys), branched-chain amino acids (Ile, Leu, Val), and His. Together, these amino acids constitute a chemical defense system centered on redox regulation, energy supply, and heavy metal chelation.

Redox buffering network of sulfur-containing amino acids. As shown in Figures 2 and 3, Met and Cys exhibited synchronized fluctuations at multiple stress time points, and their peak changes highly coincided with the activity peaks of antioxidant enzymes (GPX, SOD) reported in previous studies [55]. Met, serving as a sulfur donor for Cys and GSH synthesis [56,57], was rapidly mobilized during the early stress period (1–3 d), with its content doubling in the 50 mg/kg treatment group, reflecting a chemical preconditioning mechanism of the organism against oxidative stress. Cys is the rate-limiting substrate for GSH synthesis, and its sulfhydryl group (-SH) can directly scavenge ROS and maintain intracellular redox homeostasis through the GSH redox cycle [58,59]. This study found that the changes in Cys were particularly pronounced during the middle and late stress periods (7–10 d), and a consistent increase occurred earlier in the posterior tissue at 7–8 d, with a maximum increase of approximately 37.8% (Figure 2). These findings indicate that the posterior tissue is the primary site of Cd-induced oxidative stress and also the core site of antioxidant defense mediated by sulfur-containing amino acids.

Energy metabolism regulation by branched-chain amino acids. Branched-chain amino acids (Ile, Leu, Val) are the primary energy sources for muscle tissue. They enter the TCA cycle through catabolism to generate ATP and can also regulate mitochondrial function and the expression of antioxidant enzymes via the mTOR signaling pathway [60–64]. As shown in Figure 2, Ile increased significantly during the critical period of oxidative stress (3–4 d), with the posterior tissue reaching a maximum increase of 73.1% on day 3 and the anterior tissue reaching a maximum increase of 49.1%, indicating its role in coping with Cd stress by enhancing energy supply and antioxidant capacity. Under long-term exposure (Figure 3), Val showed opposite trends in the anterior and posterior tissues. Its content gradually decreased in the posterior tissue, possibly reflecting increased metabolic consumption, whereas its sustained increase in the anterior tissue may be associated with local metabolic regulation. These differences may reflect tissue-specific changes in energy metabolism and branched-chain amino acid utilization, but further studies are needed to verify this interpretation.

Strategic shift in histidine-mediated coordination chelation. As shown in Figures 2 and 3, His exhibited specific increases during the late stage of short-term exposure (8–10 d) and under long-term exposure (20–30 d), with the magnitude of increase in the posterior tissue being significantly greater than that in the anterior tissue. This reveals a critical strategic shift in heavy metal coordination chemistry. Previous studies have demonstrated that earthworm gut microorganisms can achieve preliminary detoxification by secreting macromolecules such as extracellular polysaccharides and α-cyclodextrin to physically encapsulate Cd ions [65,66]. However, this physical encapsulation approach has limited capacity and relatively poor stability. As the stress duration extends and microbial physical encapsulation reaches saturation, earthworms activate their endogenous chemical detoxification mechanism—synthesizing large amounts of His and utilizing the nitrogen atoms in its imidazole group to form stable five-membered chelate rings with Cd ions [67–70] thereby converting Cd ions into non-toxic or low-toxicity coordination complexes and reducing their bioavailability. The significant increase in His content suggests that earthworms may shift their detoxification strategy from microbe-mediated physical sequestration toward chemical chelation through their own metabolism. This finding provides a basis for further investigating the potential role of His in the earthworm response to Cd stress.

3.3. TOPSIS-Based Identification of Key Biomarkers and Classification of Stress Phases

By integrating the results of statistical significance tests with TOPSIS ranking contributions, the response intensity of individual amino acids to Cd stress was comprehensively evaluated based on the magnitude of their changes and their temporal and concentration-dependent dynamics. Accordingly, amino acid metabolic responses in earthworms under Cd stress were classified into three distinct stages, and stage-specific biomarkers were identified (Table 1). As shown in Figure 4, along the concentration dimension, under low-concentration Cd stress (50 mg/kg), the core responses were primarily associated with neurochemical regulation (Asp and Phe) and energy metabolism (Leu and Arg). Under moderate Cd stress (100–250 mg/kg), sulfur-containing amino acids (Cys and Met) emerged as the major responsive biomarkers, indicating broad activation of oxidative defense mechanisms. Under high Cd stress (500 mg/kg), His and Pro exhibited the most pronounced responses, suggesting a shift in detoxification strategies accompanied by the accumulation of cellular damage. As shown in Figure 4, along the temporal dimension, the first 3 d of short-term exposure were characterized predominantly by fluctuations in excitatory amino acids, which may serve as early-warning indicators of Cd-induced neurochemical disturbance. The intermediate phase (4–10 d) was characterized by coordinated changes in sulfur-containing and branched-chain amino acids, reflecting an active defense response. During long-term exposure (>10 d), a sustained increase in His emerged as a characteristic response, suggesting intensified Cd stress and increasing pressure on the organism's defense system. Collectively, this dynamic biomarker framework overcomes the limitations of conventional single-biomarker approaches and provides a more precise characterization of the intensity and progression of heavy-metal stress in soil.

Table 1. Key amino acid biomarkers and their biological significance at different stages of cadmium stress.

Stress Phase	Time Range	Concentration Range	Key Biomarkers	Biological Significance
Stress Compensatory Phase	1–3 d	50–125 mg/kg	Asp, Glu, Met	Neurotransmitter mobilization, sulfur-containing amino acid preconditioning, energy supply
Defense Reinforcement Phase	4–10 d	100–250 mg/kg	Cys, Ile, Leu, Tyr	Sulfhydryl-based antioxidant defense, energy metabolism remodeling, neurotransmitter synthesis impairment
Functional Disorder Phase	10–30 d	250–500 mg/kg	His, Val, Phe, Pro	Initiation of chelation coordination, protein degradation, accumulation of irreversible damage

During the stress compensation phase (1–3 d), TOPSIS analysis identified Asp, Glu, and Met as the major responsive biomarkers. The overall metabolic response was characterized by fluctuations in excitatory amino acids, mobilization of sulfur-containing amino acid metabolism, and the early onset of energy compensation. During this phase, Met and Ile in the posterior segment exhibited pronounced changes earlier, whereas overall amino acid homeostasis in the anterior segment remained relatively stable, with only moderate fluctuations in Asp and Glu. These findings suggest that early Cd exposure may initially induce a tissue-specific response characterized by preferential mobilization of sulfur-containing amino acid metabolism and energy compensation in the posterior segment, while relatively maintaining the homeostasis of neuroregulatory amino acids in the anterior segment. Previous studies have shown that Cd may indirectly promote ROS accumulation by disrupting mitochondrial function, antioxidant systems, and thiol homeostasis [71–75]. Met and Cys link sulfur-containing amino acid metabolism with GSH metabolism, and their dynamic changes may reflect the reallocation of sulfur-containing resources toward thiol buffering and redox defense under Cd-induced oxidative stress [76–81]. Meanwhile,

Ile increased significantly on 3–4 d, with maximum increases of 73.1% and 49.1% in the posterior and anterior segments, respectively (Figure 2). Studies have shown that BCAAs can provide carbon skeletons for processes associated with the TCA cycle through catabolism [60,82–87], suggesting that the early increase in Ile may be associated with energy compensation under Cd stress.

As the exposure was extended to 4–10 d, the metabolic response entered a phase of enhanced defense, and the key markers screened by TOPSIS shifted to Cys, Ile, Leu, and Tyr, indicating that the Cd response had expanded from rapid early compensation to multiple functional modules, including redox defense, energy metabolism, and neuro-related metabolism. Among them, the sustained response of Cys in the posterior tissue may reflect increased demands for GSH synthesis, thiol buffering, and antioxidant defense under continued Cd stress. The coordinated changes in BCAAs such as Ile and Leu may be associated with adjustments in energy metabolism, potentially providing metabolic support for active defense processes. In contrast to the enhanced defense in the later stage, Asp/Glu in the early stage gradually rebounded after an initial decline, while the responses of aromatic amino acids such as Tyr were enhanced, suggesting that the neuro-related metabolic homeostasis in the early stage began to shift from early compensatory adjustment to pronounced disturbance. Existing studies have shown that Cd can interfere with Glu neurotransmission through multiple molecular targets, including NMDA receptors, postsynaptic scaffold proteins, and excitatory amino acid transport processes [88–91]. Persistent imbalance in Glu homeostasis may further disturb Ca^{2+} homeostasis, mitochondrial function, and redox balance [92–94]. Therefore, the dynamic transition of Asp/Glu in this study is consistent to some extent with the mechanisms associated with Cd neurotoxicity, suggesting that excitatory amino acid homeostasis in the early stage may be a relatively sensitive metabolic target under continuous Cd exposure.

After further extending the exposure to 10–30 d, the metabolic response gradually entered a phase of functional disorder, and the key markers identified by TOPSIS shifted further to His, Val, Phe, and Pro, indicating that the focus of metabolic regulation had expanded from early redox buffering and energy compensation to multiple functional dimensions, including metal coordination, BCAA homeostasis, and aromatic amino acid metabolism. The sustained increase in His during the later stages of short-term exposure and throughout long-term exposure may have implications for metal coordination chemistry. The imidazole group in its side chain can coordinate metals, and Cd^{2+} can form stable metal–ligand complexes with His and His-containing ligands [95–97]. Similar His-rich structural domains are also involved in heavy metal binding and transport processes in other organisms [98,99]. Therefore, the sustained elevation of His in the later stage may reflect a gradual expansion of its defense strategy from thiol buffering and energy compensation to Cd^{2+} coordination processes [68]. Meanwhile, the persistent changes in aromatic amino acids such as Phe and Tyr under long-term, high-concentration Cd exposure may indicate further disruption of the metabolic homeostasis of neurotransmitter precursors. Phe can be converted to Tyr by phenylalanine hydroxylase (PAH), and Tyr is subsequently involved in the synthesis of catecholamine neurotransmitters [100–102]. An imbalance in Phe and Tyr may affect the precursor supply for neurotransmitters such as dopamine, potentially increasing the risk of impaired neural function. This interpretation requires further validation through measurements of PAH activity and neurotransmitter levels. Notably, at 10 d of exposure to 500 mg/kg Cd, the total amino acid content in the early stage rose to 485.69 mg/g (Figure 2), indicating that amino acid homeostasis had undergone pronounced changes under high-intensity continuous stress. This abnormal accumulation may involve imbalances in protein turnover, amino acid utilization efficiency, and stress metabolic processes, reflecting a gradual decline in the compensatory capacity of the early-stage tissue and its transition toward functional disorder.

3.4. Microbial Interactions with Amino Acid Reprogramming in the Anterior and Posterior Segments of Earthworms

3.4.1. Tissue-Specific Association Patterns Between Amino Acids and Microbiota in the Anterior and Posterior Segments

To further elucidate the potential links between host amino acid metabolism and microbial changes under Cd stress, the TOPSIS evaluation identified day 10 at 500 mg/kg Cd as the key stress condition. Spearman correlation analysis was subsequently performed between genus-level microbial abundances and the contents of 17 amino acids in the anterior and posterior segments of earthworms. The results revealed distinct amino acid-microbiota association patterns between the anterior and posterior segments (Figure S1), indicating tissue-specific associations between amino acid metabolism and microbial communities under Cd stress. The amino acid–microbe correlations and path coefficients in this study were used to describe statistical associations between variables and the direct and indirect effects specified by the model. These results primarily reflect statistical relationships; their potential causal links and underlying mechanisms require further investigation.

In the anterior segment, *Acinetobacter*, *Comamonas*, and *Escherichia* were generally positively correlated with multiple amino acids, whereas *Paracoccus* and *Pseudomonas* predominantly exhibited negative correlations. Notably, neuroregulation-related amino acids, including Asp, Glu, Phe, and Tyr, showed distinct microbial taxon-specific associations. Asp/Glu and Phe/Tyr displayed distinct correlation patterns with different microbial taxa, suggesting tissue-specific statistical associations between Cd-induced changes in neurorelated amino acids and the relative abundances of different microbial taxa. Previous studies have shown that heavy metal exposure can significantly alter the gut microbial communities of earthworms, and that gut microbiota are more sensitive to heavy metal contamination than microbial communities in the surrounding soil, indicating that the internal microenvironment of earthworms exhibits distinct responses to contamination [103]. In addition, Cd exposure can alter gut microbial taxa with metal tolerance or binding capacities, and genera such as *Pseudomonas* have been reported to be closely associated with Cd exposure [104]. Recent studies have further demonstrated that pollutant stress can simultaneously disrupt the composition of the earthworm gut microbiota, the TCA cycle, and amino acid metabolism, with certain microbial taxa showing close associations with host amino acid metabolism [105]. Therefore, the distinct associations of Asp/Glu and Phe/Tyr with different microbial taxa observed in this study may reflect a potential link between neurorelated metabolic status in the anterior tissue and changes in the local microbial community under Cd stress.

In contrast to the anterior segment, microbial–amino acid associations in the posterior segment were more strongly concentrated in detoxification-related metabolic modules. *Aeromonas*, *Comamonas*, and *Escherichia* were generally positively correlated with multiple amino acids, whereas *Bordetella*, *Herbaspirillum*, *Paracoccus*, and *Pseudomonas* predominantly exhibited negative correlations with most amino acids. In particular, the sulfur-containing amino acids Cys and Met, the branched-chain amino acids Ile, Leu, and Val, and His all exhibited distinct genus-dependent associations. These amino acids are associated with redox buffering, energy compensation, and metal coordination. Their concurrent changes with specific microbial taxa suggest that detoxification-related metabolic reprogramming in the posterior tissue may be associated with the abundance of certain microbial taxa, indicating a potential relationship between host metabolic status and the local microbial community. Cd can accumulate in the midgut and hindgut of earthworms and is accompanied by alterations in gut microbial community structure. Certain gut bacteria may also contribute to Cd adsorption and immobilization and are closely associated

with host responses involving oxidative stress and energy metabolism [106–108]. Therefore, the differential associations of Met/Cys, BCAAs, and His with microbial taxa observed in this study are consistent with the metabolic characteristics of the posterior segment associated with its stronger Cd defense capacity.

Taken together, Cd stress was associated with distinct microbe–metabolite patterns across tissues, rather than a uniform pattern throughout the earthworm, corresponding to the different physiological responses of the anterior and posterior tissues. In the anterior segment, these associations were primarily linked to changes in the homeostasis of neuroregulation-related amino acids, including Asp, Glu, Phe, and Tyr, whereas in the posterior segment, they were more closely associated with Met/Cys-mediated redox buffering, BCAA-related energy compensation, and His-related metal coordination. This consistency between microbial association patterns and host metabolic functions is in line with the high sensitivity of the earthworm gut microbiota to heavy metal exposure and its potential roles in Cd immobilization and host metabolic adaptation [109]. Therefore, tissue specificity under Cd stress may be reflected not only in the differential allocation of host amino acid resources but also in the establishment of distinct local microbiota-metabolism relationships, providing new ecological perspective for the functional division of "central protection–peripheral detoxification."

3.4.2. Coordinated Pathways Between Key Amino Acids and Microbiota and Their Tissue-Specific Differences

Path analysis further revealed pronounced tissue-specific association patterns between internal and external microbiota and key amino acids in earthworms under Cd stress (Figure 5). In the anterior segment, these associations were primarily concentrated on neuroregulation-related amino acids, including Asp, Glu, Phe, and Tyr. Among them, Glu-*Escherichia* (1.0188), Asp-*Subdoligranulum* (−0.8243), Tyr-*Gammaretrovirus* (−0.8025), and Phe-*Paracoccus* (−0.9930) exhibited relatively large direct path coefficients, indicating that microbial changes in the anterior tissue showed relatively strong path associations with excitatory and aromatic amino acid metabolism. Studies have shown that Asp and Glu are involved not only in nitrogen and energy metabolism but are also closely associated with excitatory neurotransmission, while Phe and Tyr serve as important metabolic precursors for neuroactive compounds such as catecholamines [101]. Therefore, the relatively strong path relationships between microbial nodes such as *Escherichia*, *Subdoligranulum*, *Gammaretrovirus*, and *Paracoccus* and the above-mentioned amino acids suggest that Cd-induced changes in the microbial community in the anterior tissue may be associated with disruptions in neurorelated amino acid homeostasis. This finding is consistent with the previously observed fluctuations in Asp/Glu and imbalances in Phe/Tyr in the anterior segment, further supporting that the anterior response to Cd stress is primarily centered on the maintenance and disruption of neuroregulation-related metabolic homeostasis.

In contrast, associations in the posterior segment were primarily concentrated on amino acids involved in redox defense, energy metabolism, and metal coordination, including Cys, Met, Ile, Leu, Val, and His. Among these, Cys-*Achromobacter* (−1.0584), Val-*Paracoccus* (1.1545), and His-*Paracoccus* (−1.0645) exhibited relatively strong associations. Notably, *Paracoccus* was associated with multiple key amino acids and microbial nodes, exhibiting prominent connectivity within the overall network. Previous studies have shown that Cys and Met are important components of sulfur metabolism, and that Cys can contribute to thiol-based antioxidant systems such as GSH [76]. Meanwhile, BCAAs, including Ile, Leu, and Val, may provide carbon skeletons for the TCA cycle through their catabolism, thereby supporting the increased energy demands imposed by Cd stress [110]. His contains an imidazole group with metal-coordination capacity, enabling it to participate in Cd^{2+} binding and the regulation of free metal ion activity [68]. Therefore, the later-

stage microorganisms form a more concentrated association with Cys, Met, BCAA, and His. This association pattern may involve processes such as antioxidant defense, energy metabolism, and metal homeostasis regulation, but its specific functions still need to be further verified through experiments.

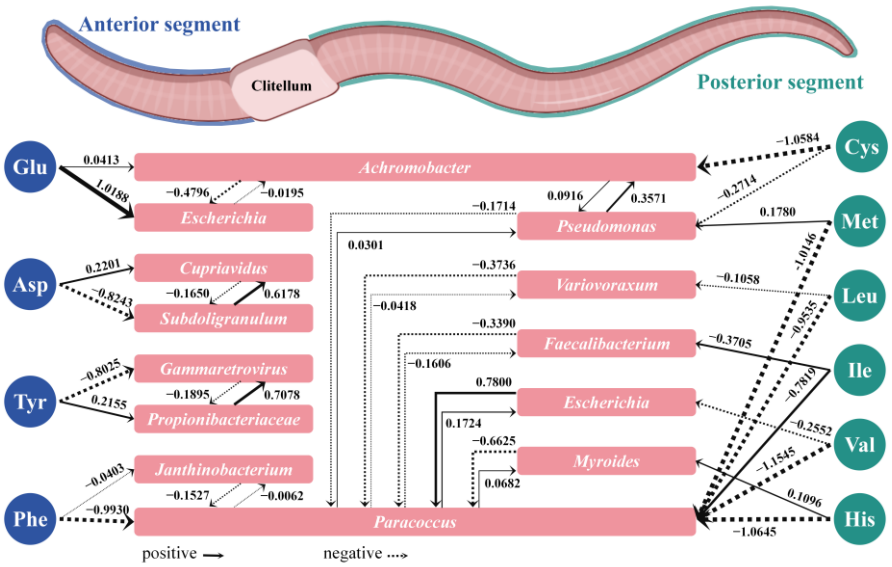


Figure 5. Synergistic pathways between amino acids and microorganisms in earthworms following stress exposure.

Overall, the anterior segment exhibited a neuroregulation-related metabolic association pattern centered on Asp, Glu, Phe, and Tyr, whereas the posterior segment displayed a defense- and detoxification-related metabolic association pattern centered on Cys, Met, BCAAs, and His. These findings further demonstrate the pronounced tissue specificity of amino acid–microbiota associations in earthworms under Cd stress. This spatial differentiation of amino acid–microbiota associations further refines the tissue-coordinated mechanism of "central protection–peripheral detoxification" under Cd stress (Figure 6). Meanwhile, this study found that the microbiota in the posterior segment showed a more concentrated association pattern with defense-related amino acids such as Cys, Met, BCAA, and His, indicating that the posterior segment's response to Cd does not rely on changes in a single metabolite. There may be an important correlation between host amino acid metabolism and local microbial communities, thereby forming a multi-level metabolic defense system encompassing redox buffering, energy compensation, and metal coordination. From an ecological perspective, tissue-specific metabolic reprogramming under Cd stress may reflect not only resource reallocation by the earthworm but also coordinated changes between internal and external microbial communities and the host's metabolic state. These findings offer insight into physiological differences in earthworm responses to soil Cd stress and a basis for identifying potential stage-specific response indicators. The associated physiological processes and their ecological significance for early warning remain to be examined in future studies.

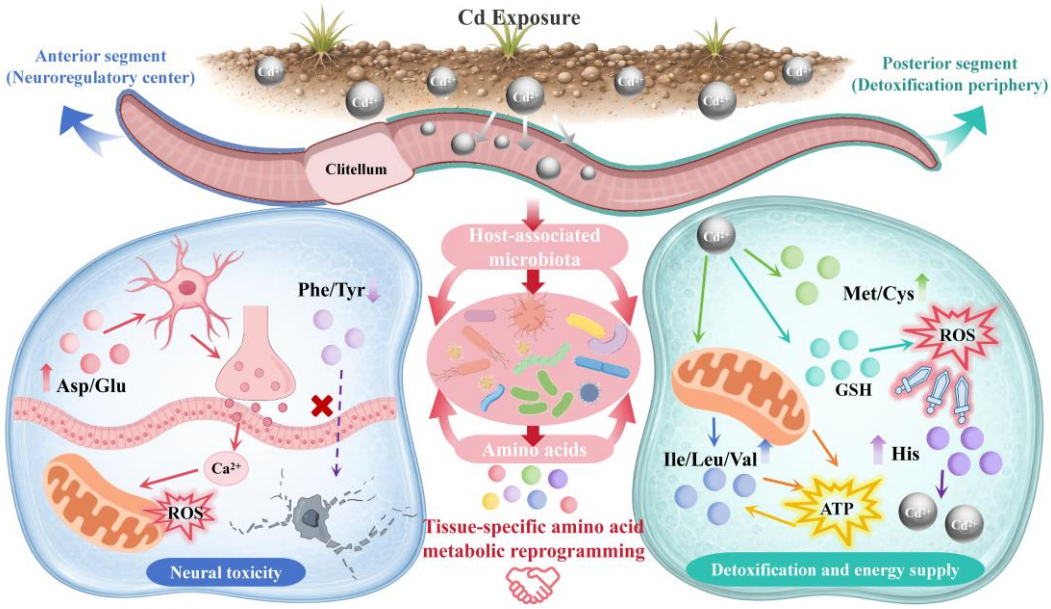


Figure 6. Tissue-Coordinated Response Mechanism of "Central Protection–Peripheral Detoxification" under Cd Stress.

4. Conclusions

This study revealed pronounced tissue-specific reprogramming of amino acid metabolism in *Eisenia fetida* under Cd stress. The anterior segment was primarily characterized by disrupted homeostasis of neuroregulation-related amino acids, including Asp, Glu, Phe, and Tyr, whereas the posterior segment exhibited differential responses of Met/Cys, BCAAs, and His, forming a multilayered defense involving redox buffering, energy compensation, and potential metal coordination. Combined with the dynamic changes and TOPSIS analysis, earthworm amino acid metabolism exhibited a stage-dependent trajectory of "stress compensation–defense reinforcement–functional disruption." Amino acid–microbiota association and path analyses further demonstrated pronounced tissue-specific differentiation in amino acid metabolism–microbiota coupling. Taken together, these findings support a tissue-coordinated response framework centered on "central protection–peripheral detoxification," providing new metabolic and ecological insights into amino acid–microbiota interactions and tissue-specific adaptive mechanisms in earthworms under Cd stress.

Supplementary Materials: The following supporting information can be downloaded at: https://www.mdpi.com/article/10.3390/antiox15111506/s1. Figure S1: Association patterns between internal and external microbiota and amino acid metabolism in earthworms under cadmium stress; Figure S2: Genus-level microbial abundance inside and outside earthworms under cadmium stress.

Author Contributions: Y.N.: Conceptualization, Data curation, Formal analysis, Funding acquisition, Investigation, Methodology, Writing—original draft. H.W.: Data curation, Formal analysis, Investigation, Methodology, Software, Writing—original draft. J.S.: Date analysis, Investigation, Methodology, Validation. J.G.: Resources. G.W.: Resources. D.Z.: Conceptualization, Funding acquisition, Project administration, Resources, Supervision, Validation, Visualization, Writing—reviewing and editing. All authors have read and agreed to the published version of the manuscript.

Funding: This work was financially supported by the National Natural Science Foundation of China (42107327), Natural Science Foundation of Heilongjiang Province (YQ2021D002), and the Science and Technology Department, Heilongjiang Province (2022ZXJ08B01-1).

Institutional Review Board Statement: Not applicable.

Informed Consent Statement: Not applicable.

Data Availability Statement: The data presented in this study are openly available in the Science Data Bank at https://doi.org/10.57760/sciencedb.00zsz.

Acknowledgments: The soil components and earthworms in the mechanism diagram of this study were generated with the assistance of Chat GPT, 26.1111.2228.0; this tool was used only for auxiliary generation of graphical components and did not participate in research design, data analysis, or interpretation of results.

Conflicts of Interest: The authors declare no conflicts of interest.

References

1. Li, S.; Fu, W.; Li, B.; Wang, Y.; Cheng, Y.; Kang, H.; Zeng, J. Insight into Cd Detoxification and Accumulation in Wheat by Foliar Application of Ferulic Acid. *Plants* **2025**, *14*, 1436. https://doi.org/10.3390/plants14101436.
2. Wu, X.P.; Mei, H.; Xu, J.W.; Ji, T.; Huang, H.; Ding, Y.; Zhu, W. A field study: Vermicompost mitigates Cd migration in soil-celery system. *Ecotoxicol. Environ. Saf.* **2026**, *309*, 119730. https://doi.org/10.1016/j.ecoenv.2026.119730.
3. Su, S.X.; Lin, M.J.; Li, K.; Lin, J.; Chen, Z. Soil aggregates as functional units for cadmium sequestration: Differential regulation by nitrogen enrichment and labile carbon inputs. *J. Hazard. Mater.* **2026**, *511*, 142196. https://doi.org/10.1016/j.jhazmat.2026.142196.
4. Li, K.; Zeng, C.; Liu, J.; Chen, Q.; Zheng, M.; Xu, Y.; Lu, C. Synergistic interactions among ramie (*Boehmeria nivea*, L.).; earthworm (*Eisenia fetida*), and soil microbials in phytoremediation on soil cadmium absorption. *J. Environ. Sci.* **2026**, *162*, 687–695. https://doi.org/https://doi.org/10.1016/j.jes.2025.06.059.
5. Ning, Y.C.; Li, Y.Z.; Guo, H.Y.; Sun, J.; Xue, J.; Xu, Y.; Li, Z.; Zou, D.; Zhou, D. Earthworm stress adaptation: The pivotal role of viruses in microplastic-cadmium co-exposure. *Appl. Soil Ecol.* **2026**, *217*, 106625. https://doi.org/10.1016/j.apsoil.2025.106625.
6. Zhang, H.Y.; Zhou, Q.Q.; Liu, R.Y.; Zhao, Z.; Liu, J.; Siddique, K.H.; Mao, H. Enhancing zinc biofortification and mitigating cadmium toxicity in soil-earthworm-spinach systems using different zinc sources. *J. Hazard. Mater.* **2024**, *476*, 135243. https://doi.org/10.1016/j.jhazmat.2024.135243.
7. Feng, Q.; Wang, X.Y.; Wang, X.; Xu, M. A bibliometric analysis and literature review of earthworms used as bio-indicators for assessing soil heavy metal pollution. *J. Environ. Sci.* **2026**, *162*, 763–773. https://doi.org/10.1016/j.jes.2025.06.052.
8. Walia, S.S.; Kaur, T. Earthworms, Their Species, and Biological Features. In *Earthworms and Vermicomposting: Species, Procedures and Crop Application*; Walia, S.S., Kaur, T., Eds.; Springer Nature: Singapore, 2024; pp. 17–36. https://doi.org/10.1007/978-981-99-8953-9_3.
9. Ning, Y.C.; Zhou, H.R.; Wang, E.Z.; Jin, C.; Yu, Y.; Cao, X.; Zhou, D. Study of cadmium (Cd)-induced oxidative stress in *Eisenia fetida* based on mathematical modelling. *Pedosphere* **2021**, *31*, 460–470. https://doi.org/10.1016/S1002-0160(20)60085-6.
10. Bollati, C.; Tosi, M.; d'Adduzio, L.; Fanzaga, M.; Burlina, A.; Zuccotti, G.; Lammi, C.; Verduci, E. Antioxidant and Anti-Inflammatory Activity of a New Formulation of Slow-Release Amino Acids in Human Intestinal Caco-2 Cells. *Antioxidants* **2025**, *14*, 271. https://doi.org/10.3390/antiox14030271.
11. Yang, M.; An, Z.W.; Xing, X.Q.; Mei, Y.; Li, H.; Tan, Z.; Li, Y.; Zhao, J.; Zhao, J.; Zhao, M.; et al. Standing at the crossroads: How does amino acids function in the crosstalk between pancreas and the kidney under exposure to, per-and polyfluoroalkyl substances? *J. Hazard. Mater.* **2025**, *496*, 139257. https://doi.org/10.1016/j.jhazmat.2025.139257.
12. Zhang, G.; Huang, S.; Wei, M.; Wu, Y.; Wang, J. Excitatory Amino Acid Transporters as Therapeutic Targets in the Treatment of Neurological Disorders: Their Roles and Therapeutic Prospects. *Neurochem. Res.* **2025**, *50*, 155. https://doi.org/10.1007/s11064-025-04400-3.
13. Chen, X.; Xie, H.; Pan, Y.; Qu, K.; Liu, Y.; Song, J.; Tan, B.; Yang, Q.; Xie, S. Arginine improves growth and health status of post-larval Litopenaeus vannamei by modulating amino acid metabolism and enhancing antioxidative defense. *Amino Acids* **2026**, *58*, 22. https://doi.org/10.1007/s00726-026-03510-8.
14. Carretero, V.J.; Ramos, E.; Segura-Chama, P.; Hernández, A.; Baraibar, A.M.; Álvarez-Merz, I.; Muñoz, F.L.; Egea, J.; Solís, J.M.; Romero, A.; et al. Non-Excitatory Amino Acids, Melatonin, and Free Radicals: Examining the Role in Stroke and Aging. *Antioxidants* **2023**, *12*, 1844. https://doi.org/10.3390/antiox12101844.

15. Kang, F.; Wei, R.; Huang, X.; Dawuda, U.K.; Xu, P.; Li, Z.; Tao, Z.; Tian, L.; Ouyang, X.; Guo, Q. The effects of typical amino acid ligands on Cd and translocation and detoxification processes in hyperaccumulator *Sedum alfredii* Hance. *J. Environ. Sci.* **2026**, *164*, 47–56. https://doi.org/https://doi.org/10.1016/j.jes.2025.09.025.
16. Oshima, T.; Ishizaka, S.; Morizono, H.; Ohe, K.; Baba, Y. Adsorption behavior of metal ions on alkylhistidine extractant impregnated resins: Effect of functional groups of histidine. *Sep. Purif. Technol.* **2013**, *114*, 11–16. https://doi.org/10.1016/j.seppur.2013.04.016.
17. Thirupathi, P.; Lee, K.H. A ratiometric fluorescent detection of Zn(II) in aqueous solutions using pyrene-appended histidine. *Bioorganic Med. Chem. Lett.* **2013**, *23*, 6811–6815. https://doi.org/10.1016/j.bmcl.2013.10.015.
18. Zhou, D.X.; Liang, X.Y.; Wang, J.H.; Wang, S.; Li, X.; Ning, Y. Study on the regulatory mechanism of the earthworm microbial community in vitro and in vivo under cadmium stress. *Environ. Pollut.* **2021**, *279*, 116891. https://doi.org/10.1016/j.envpol.2021.116891.
19. Strotmann, U.; Thouand, G.; Pagga, U.; Gartiser, S.; Heipieper, H.J. Toward the future of OECD/ISO biodegradability testing-new approaches and developments. *Appl. Microbiol. Biotechnol.* **2023**, *107*, 2073–2095. https://doi.org/10.1007/s00253-023-12406-6.
20. da Silva, L.M.; Andrade-Vieira, L.F. Ecotoxicological bioassays with terrestrial plants: A holistic view of standards guidelines, and protocols. *J. Toxicol. Environ. Health Part B* **2025**, *28*, 183–221. https://doi.org/10.1080/10937404.2024.2440876.
21. General, C. *Test No. 207: Earthworm, Acute Toxicity Tests*; OECD Guidelines for the Testing of Chemicals, Section 2; OECD Publishing: Paris, France, 1984; Volume 1, pp. 1–9.
22. General, C. *Test No. 222: Earthworm Reproduction Test (Eisenia fetida/Eisenia andrei)*; OECD Guidelines for the Testing of Chemicals, Section 2; OECD Publishing: Paris, France, 2006; Volume 1, pp. 1–18.
23. Zaltauskaite, J.; Sodiene, I. Effects of cadmium and lead on the life-cycle parameters of juvenile earthworm *Eisenia fetida*. *Ecotoxicol. Environ. Saf.* **2014**, *103*, 9–16. https://doi.org/10.1016/j.ecoenv.2014.01.036.
24. Dongxing, Z.; Yucui, N.; Jiabin, L.; Jie, D.; Guohua, R.; Bilige, S.; Yijun, L. Effects of oxidative stress reaction for the *Eisenia fetida* with exposure in Cd^{2+}. *Environ. Sci. Pollut. Res.* **2016**, *23*, 21883–21893. https://doi.org/10.1007/s11356-016-7422-6.
25. Dongxing, Z.; Yucui, N.; Congmin, J.; Liyan, L.; Xiaoli, P.; Xu, C. Correlation of the oxidative stress indices and Cd exposure using a mathematical model in the earthworm, *Eisenia fetida*. *Chemosphere* **2019**, *216*, 157–167. https://doi.org/10.1016/j.chemosphere.2018.10.117.
26. Kristensen, N.B.; Jungvid, H.; Fernández, J.A.; Pierzynowski, S.G. Absorption and metabolism of α-ketoglutarate in growing pigs. *J. Anim. Physiol. Anim. Nutr.* **2002**, *86*, 239–245. https://doi.org/https://doi.org/10.1046/j.1439-0396.2002.00380.x.
27. DeBerardinis, R.J.; Mancuso, A.; Daikhin, E.; Nissim, I.; Yudkoff, M.; Wehrli, S.; Thompson, C.B. Beyond aerobic glycolysis: Transformed cells can engage in glutamine metabolism that exceeds the requirement for protein and nucleotide synthesis. *Proc. Natl. Acad. Sci. USA* **2007**, *104*, 19345–19350. https://doi.org/10.1073/pnas.0709747104.
28. Sakatoku, A.; Ishikawa, M.; Yamazaki, K.; Nakamachi, T.; Kamachi, H.; Tanaka, D.; Nakamura, S. Molecular Identification, Characterization, and Expression Analysis of a Metallothionein Gene from *Septifer virgatus*. *Mar. Biotechnol.* **2020**, *22*, 488–497. https://doi.org/10.1007/s10126-020-09970-7.
29. Li, C. Insulin Secretion the Glutamine-Glutamate-Alpha-Ketoglutarate Axis. In *Glutamine in Clinical Nutrition*; Rajendram, R., Preedy, V.R., Patel, V.B., Eds.; Springer: New York, NY, USA, 2015; pp. 239–254. https://doi.org/10.1007/978-1-4939-1932-1_19.
30. Zhang, L.H.; Zhou, L.N.; Han, L.S.; Zhao, C.; Norton, J.M.; Li, H.; Hu, F.; Xu, L. Benzo(a)pyrene inhibits the accumulation and toxicity of cadmium in subcellular fractions of *Eisenia fetida*. *Chemosphere* **2019**, *219*, 740–747. https://doi.org/10.1016/j.chemosphere.2018.12.083.
31. Chagin, A.S. Effectors of mTOR-autophagy pathway: Targeting cancer, affecting the skeleton. *Curr. Opin. Pharmacol.* **2016**, *28*, 1–7. https://doi.org/https://doi.org/10.1016/j.coph.2016.02.004.
32. Hussain, N.; Chatterjee, S.K.; Maiti, T.K.; Goswami, L.; Das, S.; Deb, U.; Bhattacharya, S.S. Metal induced non-metallothionein protein in earthworm: Anew pathway for cadmium detoxification in chloragogenous tissue. *J. Hazard. Mater.* **2021**, *401*, 123357. https://doi.org/10.1016/j.jhazmat.2020.123357.
33. Jiang, X.F.; Wang, X.W.; Kah, M.; Li, M. Environmentally relevant concentrations of microplastics from agricultural mulch and cadmium negatively impact earthworms by triggering neurotoxicity and disrupting homeostasis. *J. Hazard. Mater.* **2024**, *476*, 135158. https://doi.org/10.1016/j.jhazmat.2024.135158.
34. Sizmur, T.; Hodson, M.E. Do earthworms impact metal mobility and availability in soil?—A review. *Environ. Pollut.* **2009**, *157*, 1981–1989. https://doi.org/10.1016/j.envpol.2009.02.029.

35. Ahmad, I.; Ahmed, I.; Dar, N.A. Dietary valine improved growth, immunity, enzymatic activities and expression of TOR signaling cascade genes in rainbow trout, *Oncorhynchus mykiss* fingerlings. *Sci. Rep.* **2021**, *11*, 22089. https://doi.org/10.1038/s41598-021-01142-4.
36. Cao, Q.Q.; Zhao, J.; He, L.J.; Zhang, T.; Feng, L.; Jiang, W.; Wu, P.; Zhao, J.; Liu, H.; Jiang, J. Evaluation of the dietary L-valine on fish growth and intestinal health after infection with *Aeromonas veronii*. *Aquaculture* **2024**, *580*, 740294. https://doi.org/10.1016/j.aquaculture.2023.740294.
37. Martinez-Hernandez, A.; Bell, K.P.; Norenberg, M.D. Glutamine Synthetase: Glial Localization in Brain. *Science* **1977**, *195*, 1356–1358. https://doi.org/10.1126/science.14400.
38. Pehrson, A.L.; Sanchez, C. Altered γ-aminobutyric acid neurotransmission in major depressive disorder: A critical review of the supporting evidence and the influence of serotonergic antidepressants. *Drug Des. Dev. Ther.* **2015**, *9*, 603–624. https://doi.org/10.2147/DDDT.S62912.
39. Wang, H.; Peng, R.Y.; Zhao, L.; Wang, S.; Gao, Y.; Wang, L.; Zuo, H.; Dong, J.; Xu, X.; Zhou, H.; et al. The relationship between NMDA receptors and microwave-induced learning and memory impairment: Along-term observation on Wistar rats. *Int. J. Radiat. Biol.* **2015**, *91*, 262–269. https://doi.org/10.3109/09553002.2014.988893.
40. Lai, K.; Pritišanac, I.; Liu, Z.-Q.; Liu, H.-W.; Gong, L.-N.; Li, M.-X.; Lu, J.-F.; Qi, X.; Xu, T.-L.; Forman-Kay, J.; et al. Glutamate acts on acid-sensing ion channels to worsen ischaemic brain injury. *Nature* **2024**, *631*, 826–834. https://doi.org/10.1038/s41586-024-07684-7.
41. Andersen, J.V.; Schousboe, A.; Verkhratsky, A. Astrocyte energy and neurotransmitter metabolism in Alzheimer's disease: Integration of the glutamate/GABA-glutamine cycle. *Prog. Neurobiol.* **2022**, *217*, 102331. https://doi.org/10.1016/j.pneurobio.2022.102331.
42. Madsen, T.E.; Liu, S.M. Amino acid neurotransmitters and prognosis after stroke: Nutrition as a modifiable factor to improve stroke outcomes. *Am. J. Clin. Nutr.* **2023**, *118*, 737–738. https://doi.org/10.1016/j.ajcnut.2023.07.022.
43. Martinez-Lozada, Z.; Ortega, A. Milestone Review: Excitatory amino acid transporters—Beyond their expected function. *J. Neurochem.* **2023**, *165*, 457–466. https://doi.org/10.1111/jnc.15809.
44. Wojtas, A.; Bysiek, A.; Wawrzczak-Bargiela, A.; Szych, Z.; Majcher-Maślanka, I.; Herian, M.; Maćkowiak, M.; Gołembiowska, K. Effect of Psilocybin and Ketamine on Brain Neurotransmitters, Glutamate Receptors, DNA and Rat Behavior. *Int. J. Mol. Sci.* **2022**, *23*, 6713. https://doi.org/10.3390/ijms23126713.
45. Parsons, M.P.; Raymond, L.A. Extrasynaptic NMDA Receptor Involvement in Central Nervous System Disorders. *Neuron* **2014**, *82*, 279–293. https://doi.org/10.1016/j.neuron.2014.03.030.
46. Sattler, R.; Xiong, Z.; Lu, W.-Y.; Hafner, M.; MacDonald, J.F.; Tymianski, M. Specific Coupling of NMDA Receptor Activation to Nitric Oxide Neurotoxicity by PSD-95 Protein. *Science* **1999**, *284*, 1845–1848. https://doi.org/10.1126/science.284.5421.1845.
47. Qiu, J.; Tan, Y.W.; Hagenston, A.M.; Martel, M.-A.; Kneisel, N.; Skehel, P.A.; Wyllie, D.J.A.; Bading, H.; Hardingham, G.E. Mitochondrial calcium uniporter Mcu controls excitotoxicity and is transcriptionally repressed by neuroprotective nuclear calcium signals. *Nat. Commun.* **2013**, *4*, 2034. https://doi.org/10.1038/ncomms3034.
48. Yu, S.P.; Jiang, M.Q.; Shim, S.S.; Pourkhodadad, S.; Wei, L. Extrasynaptic NMDA receptors in acute and chronic excitotoxicity: Implications for preventive treatments of ischemic stroke and late-onset Alzheimer's disease. *Mol. Neurodegener.* **2023**, *18*, 43. https://doi.org/10.1186/s13024-023-00636-1.
49. Azizi, S.A. Monoamines: Dopamine, Norepinephrine, and Serotonin, Beyond Modulation, "Switches" That Alter the State of Target Networks. *Neuroscientist* **2022**, *28*, 121–143. https://doi.org/10.1177/1073858420974336.
50. Zhang, S.N.; Hinck, A.P.; Fitzpatrick, P.F. The Amino Acid Specificity for Activation of Phenylalanine Hydroxylase Matches the Specificity for Stabilization of Regulatory Domain Dimers. *Biochemistry* **2015**, *54*, 5167–5174. https://doi.org/10.1021/acs.biochem.5b00616.
51. Harding, C.O.; Winn, S.R.; Gibson, K.M.; Arning, E.; Bottiglieri, T.; Grompe, M. Pharmacologic inhibition of L-tyrosine degradation ameliorates cerebral dopamine deficiency in murine phenylketonuria (PKU). *J. Inherit. Metab. Dis.* **2014**, *37*, 735–743. https://doi.org/10.1007/s10545-013-9675-2.
52. Homma, D.; Katoh, S.; Tokuoka, H.; Ichinose, H. The role of tetrahydrobiopterin and catecholamines in the developmental regulation of tyrosine hydroxylase level in the brain. *J. Neurochem.* **2013**, *126*, 70–81. https://doi.org/10.1111/jnc.12287.
53. Dilmukhametova, L.K.; Pronina, T.S.; Volina, E.V.; Ugryumov, M.V. The regulation of compensatory dopamine synthesis in the arcuate nucleus of rats. *Neurochem. J.* **2014**, *8*, 168–177. https://doi.org/10.1134/S1819712414030039.
54. Scholl-Bürgi, S.; Schroecksnadel, S.; Jenny, M.; Karall, D.; Fuchs, D. Chronic Immune Stimulation May Cause Moderate Impairment of Phenylalanine 4-hydroxylase. *Pteridines* **2011**, *22*, 120–125. https://doi.org/10.1515/pteridines.2011.22.1.120.

55. Ning, Y.C.; Bao, J.X.; Xue, J.Q.; Qu, B.W.; Gong, J.Y.; Wang, C.; Zhou, D.X. Insight into key microbes drive the fatty acid β-oxidation pathway and longevity regulation pathway-worm: Unraveling earthworm detoxification mechanisms and potential remediation strategies under microplastic-cadmium co-exposure. *Chem. Eng. J.* **2026**, *546*, 180096. https://doi.org/10.1016/j.cej.2026.180096.
56. Xia, C.; Peng, P.; Zhang, W.; Xing, X.; Jin, X.; Du, J.; Peng, W.; Hao, F.; Zhao, Z.; Dong, K.; et al. Methionine-SAM metabolism-dependent ubiquinone synthesis is crucial for ROS accumulation in ferroptosis induction. *Nat. Commun.* **2024**, *15*, 8971. https://doi.org/10.1038/s41467-024-53380-5.
57. Ma, Q.X.; Kuzyakov, Y.; Pan, W.K.; Tang, S.; Chadwick, D.R.; Wen, Y.; Hill, P.W.; Macdonald, A.; Ge, T.; Si, L.; et al. Substrate control of sulphur utilisation and microbial stoichiometry in soil: Results of ^{13}C, ^{15}N, ^{14}C, and ^{35}S quad labelling. *ISME J.* **2021**, *15*, 3148–3158. https://doi.org/10.1038/s41396-021-00999-7.
58. Hameed, S.; Nan, J.R.; Zeng, X.; Xiong, H. Boosting the efficacy of pollutant-dye photodegradation, antibacterial, and anti-persister activity by distorted perovskite BFONPs. *Colloids Surf. B Biointerfaces* **2026**, *257*, 115173. https://doi.org/10.1016/j.colsurfb.2025.115173.
59. Ji, T.; Zheng, L.; Wu, J.; Duan, M.; Liu, Q.; Liu, P.; Shen, C.; Liu, J.; Ye, Q.; Wen, J.; et al. The thioesterase APT1 is a bidirectional-adjustment redox sensor. *Nat. Commun.* **2023**, *14*, 2807. Correction in *Nat. Commun.* **2023**, *14*, 4738. https://doi.org/10.1038/s41467-023-38464-y.
60. Sivanand, S.; Vander Heiden, M.G. Emerging Roles for Branched-Chain Amino Acid Metabolism in Cancer. *Cancer Cell* **2020**, *37*, 147–156. https://doi.org/10.1016/j.ccell.2019.12.011.
61. Wang, W.Y.; Cui, J.Y.; Ma, H.; Lu, W.; Huang, J. Targeting Pyrimidine Metabolism in the Era of Precision Cancer Medicine. *Front. Oncol.* **2021**, *11*, 684961. https://doi.org/10.3389/fonc.2021.684961.
62. Hinkle, J.S.; Rivera, C.N.; Vaughan, R.A. Branched-Chain Amino Acids and Mitochondrial Biogenesis: An Overview and Mechanistic Summary. *Mol. Nutr. Food Res.* **2022**, *66*, 2200109. https://doi.org/10.1002/mnfr.202200109.
63. Huffman, K.M.; Shah, S.H.; Stevens, R.D.; Bain, J.R.; Muehlbauer, M.; Slentz, C.A.; Tanner, C.J.; Kuchibhatla, M.; Houmard, J.A.; Newgard, C.B.; et al. Relationships Between Circulating Metabolic Intermediates and Insulin Action in Overweight to Obese, Inactive Men and Women. *Diabetes Care* **2009**, *32*, 1678–1683. https://doi.org/10.2337/dc08-2075.
64. Zhang, L.; Han, J.Q. Branched-chain amino acid transaminase 1 (BCAT1) promotes the growth of breast cancer cells through improving mTOR-mediated mitochondrial biogenesis and function. *Biochem. Biophys. Res. Commun.* **2017**, *486*, 224–231. https://doi.org/10.1016/j.bbrc.2017.02.101.
65. Xu, Z.N.; Yang, Z.F.; Zhu, T.; Shu, W.; Geng, L. Ecological improvement of antimony and cadmium contaminated soil by earthworm *Eisenia fetida*: Soil enzyme and microorganism diversity. *Chemosphere* **2021**, *273*, 129496. https://doi.org/10.1016/j.chemosphere.2020.129496.
66. Rashid, M.I.; Mujawar, L.H.; Shahzad, T.; Almeelbi, T.; Ismail, I.M.; Oves, M. Bacteria and fungi can contribute to nutrients bioavailability and aggregate formation in degraded soils. *Microbiol. Res.* **2016**, *183*, 26–41. https://doi.org/10.1016/j.micres.2015.11.007.
67. Fang, L.C.; Yang, S.S.; Huang, Q.Y.; Xue, A.; Cai, P. Biosorption mechanisms of Cu(II) by extracellular polymeric substances from *Bacillus subtilis*. *Chem. Geol.* **2014**, *386*, 143–151. https://doi.org/10.1016/j.chemgeo.2014.08.017.
68. Stevenson, B.C.; Berden, G.; Martens, J.; Oomens, J.; Armentrout, P. Determining gas-phase chelation of zinc, cadmium, and copper cations with HisHis dipeptide using action spectroscopy and theoretical calculations. *Int. J. Mass Spectrom.* **2024**, *495*, 117154. https://doi.org/10.1016/j.ijms.2023.117154.
69. Stevenson, B.C.; Martens, J.; Berden, G.; Oomens, J.; Schäfer, M.; Armentrout, P.B. IRMPD Spectroscopic and Theoretical Structural Investigations of Zinc and Cadmium Dications Bound to Histidine Dimers. *J. Phys. Chem. A* **2020**, *124*, 10266–10276. https://doi.org/10.1021/acs.jpca.0c08861.
70. Danielsen, E.; Bauer, R.; Hemmingsen, L.; Bjerrum, M.J.; Butz, T.; Tröger, W.; Canters, G.W.; Blaauwen, T.D.; Van Pouderoyen, G. Structure of Metal Site in Cd-Substituted His117Gly Mutant of Azurin with and without Addition of Imidazole Derivatives. *Eur. J. Biochem.* **1995**, *233*, 554–560. https://doi.org/https://doi.org/10.1111/j.1432-1033.1995.554_2.x.
71. Isaev, N.K.; Stelmashook, E.; Genrikhs, E.E.; Onishchenko, G.E. Interaction between mitophagy, cadmium and zinc. *J. Trace Elem. Med. Bio* **2023**, *79*, 127230. https://doi.org/10.1016/j.jtemb.2023.127230.
72. Kumar, R.; Chinala, A.; Gullapalli, R.R. Understanding molecular mechanisms driving cadmium-induced mitochondrial dysfunction in human metabolic liver disease. *Environ. Toxicol. Pharmacol.* **2026**, *122*, 104943. https://doi.org/10.1016/j.etap.2026.104943.
73. Nguyen, K.C.; Rippstein, P.; Tayabali, A.F.; Willmore, W.G. Mitochondrial Toxicity of Cadmium Telluride Quantum Dot Nanoparticles in Mammalian Hepatocytes. *Toxicol. Sci.* **2015**, *146*, 31–42. https://doi.org/10.1093/toxsci/kfv068.
74. Thévenod, F.; Lee, W.-K.; Garrick, M.D. Corrigendum: Iron and Cadmium Entry Into Renal Mitochondria: Physiological and Toxicological Implications. *Front. Cell Dev. Biol.* **2021**, *9*, 687810. https://doi.org/10.3389/fcell.2021.687810.

75. Tian, J.L.; Li, Z.C.; Wang, L.Y.; Qiu, D.; Zhang, X.; Xin, X.; Cai, Z.; Lei, B. Metabolic signatures for safety assessment of low-level cadmium exposure on human osteoblast-like cells. *Ecotoxicol. Environ. Safe* **2021**, *207*, 111257. https://doi.org/10.1016/j.ecoenv.2020.111257.
76. Chen, G.; Fan, J.Y.; Xu, Y.; Su, P.; Yao, M.; He, X.; Zhang, C.; Zhang, C.; Gao, P.; Zhu, L. Meta-analysis of endocrine-disrupting chemical effects on earthworm functional traits. *Environ. Res.* **2025**, *272*, 121208. https://doi.org/10.1016/j.envres.2025.121208.
77. Glorieux, C.; Liu, S.H.; Trachootham, D.; Huang, P. Targeting ROS in cancer: Rationale and strategies. *Nat. Rev. Drug Discov.* **2024**, *23*, 583–606. https://doi.org/10.1038/s41573-024-00979-4.
78. Martínez, Y.; Li, X.; Liu, G.; Bin, P.; Yan, W.; Más, D.; Valdivié, M.; Hu, C.-A.A.; Ren, W.; Yin, Y. The role of methionine on metabolism, oxidative stress, and diseases. *Amino Acids* **2017**, *49*, 2091–2098. https://doi.org/10.1007/s00726-017-2494-2.
79. Tassinari, V.; Jia, W.; Chen, W.L.; Candi, E.; Melino, G. The methionine cycle and its cancer implications. *Oncogene* **2024**, *43*, 3483–3488. https://doi.org/10.1038/s41388-024-03122-0.
80. Wanders, D.; Hobson, K.; Ji, X.M. Methionine Restriction and Cancer Biology. *Nutrients* **2020**, *12*, 684. https://doi.org/10.3390/nu12030684.
81. Zhang, H.F.; Geltink, R.I.K.; Parker, S.J.; Sorensen, P.H. Transsulfuration, minor player or crucial for cysteine homeostasis in cancer. *Trends Cell Biol.* **2022**, *32*, 800–814. https://doi.org/10.1016/j.tcb.2022.02.009.
82. Chen, M.H.; Li, X.J.; Fan, R.F.; Yang, J.; Jin, X.; Hamid, S.; Xu, S. Cadmium induces BNIP3-dependent autophagy in chicken spleen by modulating miR-33-AMPK axis. *Chemosphere* **2018**, *194*, 396–402. https://doi.org/10.1016/j.chemosphere.2017.12.026.
83. Xia, Y.; Zhang, Y.M.; Zhang, J.T.; Du, Y.; Wang, Y.; Xu, A.; Li, S. Cadmium exposure induces necroptosis of porcine spleen via ROS-mediated activation of STAT1/RIPK3 signaling pathway. *Environ. Mol. Mutagen.* **2023**, *64*, 382–392. https://doi.org/10.1002/em.22565.
84. Zhao, H.S.; Sun, D.; Wang, S.; Liu, Y.; Zhao, X.; Tian, W.; Dou, X.; Liu, J.; Xu, J.; Peng, L.; et al. Branched-chain amino acids contribute to diabetic kidney disease progression via PKM2-mediated podocyte metabolic reprogramming and apoptosis. *Nat. Commun.* **2025**, *16*, 7846. https://doi.org/10.1038/s41467-025-62890-9.
85. Fu, Y.D.; Wang, Y.; Ren, H.M.; Guo, X.; Han, L. Branched-chain amino acids and the risks of dementia, Alzheimer's disease, and Parkinson's disease. *Front. Aging Neurosci.* **2024**, *16*, 1369493. https://doi.org/10.3389/fnagi.2024.1369493.
86. Kandy, S.K.; Nimonkar, M.M.; Dash, S.S.; Mehta, B.; Markandeya, Y.S. Astaxanthin Protection against Neuronal Excitotoxicity via Glutamate Receptor Inhibition and Improvement of Mitochondrial Function. *Mar. Drugs* **2022**, *20*, 645. https://doi.org/10.3390/md20100645.
87. Munoz-Pinto, M.F.; Candeias, E.; Melo-Marques, I.; Esteves, A.R.; Maranha, A.; Magalhães, J.D.; Carneiro, D.R.; Sant'aNna, M.; Pereira-Santos, A.R.; E Abreu, A.; et al. Gut-first Parkinson's disease is encoded by gut dysbiome. *Mol. Neurodegener.* **2024**, *19*, 78. https://doi.org/10.1186/s13024-024-00766-0.
88. Tu, Y.C.; Yang, Y.C.; Kuo, C.C. Modulation of NMDA channel gating by Ca^{2+} and Cd^{2+} binding to the external pore mouth. *Sci. Rep.* **2016**, *6*, 37029. https://doi.org/10.1038/srep37029.
89. Shen, Z.; Sun, D.X.; Savastano, A.; Varga, S.J.; Cima-Omori, M.-S.; Becker, S.; Honigmann, A.; Zweckstetter, M. Multivalent Tau/PSD-95 interactions arrest in vitro condensates and clusters mimicking the postsynaptic density. *Nat. Commun.* **2023**, *14*, 6839. https://doi.org/10.1038/s41467-023-42295-2.
90. Srivastava, A.; Kumari, A.; Jagdale, P.; Ayanur, A.; Pant, A.B.; Khanna, V.K. Author Correction: Potential of Quercetin to Protect Cadmium Induced Cognitive Deficits in Rats by Modulating NMDA-R Mediated Downstream Signaling and PI3K/AKT—Nrf2/ARE Signaling Pathways in Hippocampus. *NeuroMolecular Med.* **2023**, *25*, 660. https://doi.org/10.1007/s12017-023-08765-y.
91. Tong, J.; Liu, Y.; Wu, W.L.; Wang, Q.; Yang, H.; Li, J.; Gao, Z.; Liu, W.; Liu, J.; Chazot, P.; et al. PPT1 selectively depalmitoylates GAP43 to regulate neuronal excitability and cognitive function. *Sci. Adv.* **2026**, *12*, eaeb4675. https://doi.org/10.1126/sciadv.aeb4675.
92. Sakaba, T. Two Ca^{2+}-dependent steps controlling synaptic vesicle fusion and replenishment at the cerebellar basket cell terminal. *Neuron* **2008**, *57*, 406–419. https://doi.org/10.1016/j.neuron.2007.11.029.
93. Sun, J.; Pang, Z.P.; Qin, D.; Fahim, A.T.; Adachi, R.; Südhof, T.C. A dual-Ca^{2+}-sensor model for neurotransmitter release in a central synapse. *Nature* **2007**, *450*, 676–682. https://doi.org/10.1038/nature06308.
94. Wadel, K.; Neher, E.; Sakaba, T. The coupling between synaptic vesicles and Ca^{2+} channels determines fast neurotransmitter release. *Neuron* **2007**, *53*, 563–575. https://doi.org/10.1016/j.neuron.2007.01.021.
95. Walker, S.K.; Stevenson, B.C.; Yang, F.; Jones, R.M.; Berden, G.; Martens, J.; Oomens, J.; Armentrout, P. Structural characterizations of histidine-containing tripeptides complexed with zinc and cadmium dications using IRMPD spectroscopy and theoretical calculations. *Int. J. Mass Spectrom.* **2024**, *503*, 117281. https://doi.org/10.1016/j.ijms.2024.117281.

96. Zhao, H.X.; Wang, L.S.; Zhao, F.J.; Wu, L.; Liu, A.; Xu, W. SpHMA1 is a chloroplast cadmium exporter protecting photochemical reactions in the Cd hyperaccumulator Sedum plumbizincicola. *Plant Cell Environ.* **2019**, *42*, 1112–1124. https://doi.org/10.1111/pce.13456.
97. Zhao, H.X.; Wu, X.T.; Ren, H.X.; Xu, W. Functional analysis of SpHMA1 N-terminus in yeast: Regulation of cadmium (Cd) transport by his-rich motifs. *Gene* **2025**, *971*, 149809. https://doi.org/10.1016/j.gene.2025.149809.
98. Chowdhury, D.; Hell, J.W. C^{2+}/Calmodulin Binding to PSD-95 Downregulates Its Palmitoylation and AMPARs in Long-Term Depression. *Front. Synaptic Neurosci.* **2019**, *11*, 6. https://doi.org/10.3389/fnsyn.2019.00006.
99. Vallejo, D.; Codocedo, J.F.; Inestrosa, N.C. Posttranslational Modifications Regulate the Postsynaptic Localization of PSD-95. *Mol. Neurobiol.* **2017**, *54*, 1759–1776. https://doi.org/10.1007/s12035-016-9745-1.
100. Harrison, B.J.; Olver, J.S.; Norman, T.R.; Nathan, P.J. Effects of serotonin and catecholamine depletion on interleukin-6 activation and mood in human volunteers. *Hum. Psychopharmacol. Clin. Exp.* **2002**, *17*, 293–297. https://doi.org/https://doi.org/10.1002/hup.414.
101. Samaniego, M.I.A.; Arias-Almeida, B.; León-Piñeiros, A.; Figueroa, J.G.; Vargas-Freire, A.; López, M.; Solano-Cueva, N.; Collantes, J.C.; Huiracocha-Tutiven, M.D.L.; Bigoni-Ordóñez, G.D.; et al. Phenylalanine-tyrosine-catecholamine axis disorders: Pathways, molecular diagnosis, therapeutics, and emerging translational monitoring technologies. *Front. Mol. Bio Sci.* **2026**, *13*, 1767655. https://doi.org/10.3389/fmolb.2026.1767655.
102. Hassan, M.R.; Omran, Z.S.; AL-Ghanimi, A.H. The Relationship between Cadmium and Tyrosine Hydroxylase Activity in Patients with Attention Deficit Hyperactivity Disorder (ADHD). *Karbala J. Med.* **2025**, *18*, 3023. https://doi.org/10.70863/karbalajm.v18i2.4938.
103. Liu, P.; Yang, Y.; Li, M. Responses of soil and earthworm gut bacterial communities to heavy metal contamination. *Environ. Pollut.* **2020**, *265*, 114921. https://doi.org/10.1016/j.envpol.2020.114921.
104. Šrut, M.; Menke, S.; Höckner, M.; Sommer, S. Earthworms and cadmium—Heavy metal resistant gut bacteria as indicators for heavy metal pollution in soils? *Ecotoxicol. Environ. Saf.* **2019**, *171*, 843–853. https://doi.org/10.1016/j.ecoenv.2018.12.102.
105. Qiao, Z.; Huang, Q.; Li, D.; Zhang, H.; Zhang, W. Co-exposure to decabromodiphenyl ethane and cadmium disrupts gut homeostasis in earthworms (*Eisenia fetida*): Insights from microbiome-metabolome analysis. *Appl. Soil Ecol.* **2026**, *218*, 106680. https://doi.org/https://doi.org/10.1016/j.apsoil.2025.106680.
106. Wu, Y.; Chen, C.; Wang, G.; Xiong, B.; Zhou, W.; Xue, F.; Qi, W.; Qiu, C.; Liu, Z. Mechanism underlying earthworm on the remediation of cadmium-contaminated soil. *Sci. Total Environ.* **2020**, *728*, 138904. https://doi.org/10.1016/j.scitotenv.2020.138904.
107. Xu, Q.; Shi, Y.; Ke, L.; Qian, L.; Zhou, X.; Shao, X. Ciprofloxacin enhances cadmium toxicity to earthworm *Eisenia fetida* by altering the gut microorganism composition. *Environ. Pollut.* **2023**, *333*, 122106. https://doi.org/10.1016/j.envpol.2023.122106.
108. Xu, B.; Chu, T.; Zhang, R.; Yang, R.; Zhu, M.; Guo, F.; Zan, S. Earthworm gut bacteria facilitate cadmium immobilization through the formation of CdS nanoparticles. *Chemosphere* **2024**, *361*, 142453. https://doi.org/https://doi.org/10.1016/j.chemosphere.2024.142453.
109. Zhang, J.; Liu, Z.; Wang, X.; Ai, S.; Li, J.; Cheng, H.; Wang, X. The multilayered toxic effects of cadmium on earthworms are driven by both cadmium content soil properties: The potential mediating role of microbiota. *J. Clean. Prod.* **2026**, *572*, 148907. https://doi.org/https://doi.org/10.1016/j.jclepro.2026.148907.
110. Wang, H.; Feng, L.; Pei, Z.; Zhao, J.; Lu, S.; Lu, W. Gut microbiota metabolism of branched-chain amino acids and their metabolites can improve the physiological function of aging mice. *Aging Cell* **2025**, *24*, e14434. https://doi.org/https://doi.org/10.1111/acel.14434.

Disclaimer/Publisher's Note: The statements, opinions and data contained in all publications are solely those of the individual author(s) and contributor(s) and not of MDPI and/or the editor(s). MDPI and/or the editor(s) disclaim responsibility for any injury to people or property resulting from any ideas, methods, instructions or products referred to in the content.